Dear Editor and Reviewer,

We would like to thank you for accurately reading and commenting the manuscript, and suggesting how to improve it. Answers to your comments are given in details hereafter. We hope that you will find them satisfactory. All authors agree with the modifications made to the manuscript.
Reviewer comments are in bold, and are followed by our response (in blue) that includes changes and/or additions to the text.

For the authors,
Dorotea Iovino

Answer to **Referee #1**

General comments
This paper presents a summary of the basic performance for a _ten year run of a new 1/16th global model, which is to be employed for operational ocean forecasts.
Some performance comparisons are made with a similar 1/4 degree configuration of the model.
Overall I thought it was a well written paper which presented some interesting results.
Most of the analyses are fairly standard, but to me this is as one would expect for a system definition paper.
My key comments are the paper could make better use of the 1/4 degree parallel experiments they use and describe in places. For example:
* It is key to emphasize that resolution is not a panacea – there are many atmospheric forcing set errors, and errors due to limited physics, i.e. parameterisation, e.g. mixing in particular. There may also be error cancellation, e.g. a bias might get worse due to removing a cancelling error, e.g. with ocean forcing set errors, by increasing resolution.

We do agree that high horizontal resolution is not a panacea for all ocean modelling problems and it does not guarantee that all undesirable characteristics of our models are ameliorated. In fact, a number of prominent biases and model errors persist, or even worsen, despite increases in model resolution. The increase in horizontal and vertical resolutions needs to be accompanied by improved modelling of relevant physical processes at the appropriate scale. Model parameterizations that have been developed for coarse resolutions mat not be ideal for considerably finer spatial-scales and may need to be revised, requiring model developments. However, the finer resolution remains one possible way in which model capabilities can be enhanced, thanks to the explicit solution of eddies. In this paper, we want to document if and how an "eddy-resolving" ocean model resolution impacts the simulation of large-scale ocean variability with respect to an eddy-permitting configuration. We do believe that our GLOB16 results, in accordance to the current literature, provide compelling evidence that an eddying ocean component can significantly impact the simulation of the large-scale ocean dynamics. We modified the Introduction to account for this comment: "Although the increase of resolution does not necessarily lead *per se* to an improved representation of the ocean general circulation, the aim of this work is to evaluate the effect of the explicit solution of eddy dynamics at low- and mid- latitudes on the large-scale dynamics of a high-resolution global ocean model, compared to a coarser resolution configuration".

* I would ideally prefer to see many more comparison sub-plots for existing figures to identify differences of the 1/12th compared to the 1/4 twin run so we can see how many of the features you describe are common to both 1/4 and 1/12 and how many are really down to
We agree with the referee that a more detailed comparison between GLOB16 and GLOB4 can definitely improve the manuscript. To present a more complete comparison with GLOB4, we modified subplots and/or add text in any relevant part of section 3, trying not to alter too much the manuscript structure or increase its length.

* The reader ideally needs to know exactly which parameters and config settings are different for the 1/4 degree run compared to the 1/12th run. For example, is it the same version of NEMO, you mention it has level vertical levels so some differences could be due to vertical rather than spatial resolution. Also what coefficient for isopycnal mixing on tracers do you use at 1/4 (as the 1/4 simulation and biases are quite sensitive to this)?
We added the key differences in parameters and configuration settings at the end of section 2.

Minor comments:
Line 42-43 – I think it may depend on the definition but is there not a factor of pi between the Rossby radius (based on wave number) and eddy scale? This makes a difference as one only needs two grid cells per Rossby radius to get 6 cells per eddy. This would be worth clarifying?
The direct relation between the Rossby radius, R, and the baroclinic Rossby wavelength, λ, is R = λ/2π. The grid spacing Δ has to satisfy Δ < R, and then 2πΔ < λ, following the traditional criteria for resolving a wave on a discrete grid. Nevertheless, Hallberg (2013) considered a 2Δ < R criteria.
In order to clarify this, we modified the text in section 1 and added the following lines:
"Hallberg (2013) showed the model horizontal resolution required to resolve the first baroclinic deformation radius with two grid points, based on a Mercator grid. From his analysis, 1/4° Mercator spacing is insufficient to resolve mesoscale eddies that have a typical scale of 50 km at mid-latitudes."

Line 53 – should you mention 'often (wrongly) termed eddy resolving' in view of the fact you go on to state they are not eddy resolving at high latitudes as shown by Hallberg (2013)?
We apologise for pointing out that we did find this specific text neither in line 53 nor elsewhere in the manuscript. As reported by emails, we did not detect a direct correspondence between some line numbers indicated by the Referee's comments and the line numbers reported in the pdf file (available online http://www.geosci-model-dev-discuss.net/gmd-2015-268/gmd-2015-268.pdf). However, following this comment, we highlighted in the introduction that GLOB16 and configurations with comparable horizontal resolution do not resolve mesoscale globally, and are only eddy-permitting north of a certain latitude and over shelf regions. The test now reads "Resolving mesoscale eddy variability remains anyway elusive at higher latitudes. For example, in the Arctic Ocean where the first Rossby radius decreases down to few kilometres on the continental shelf or in weakly stratified regions, typical eddy-resolving resolution does only permit eddies at best (Nurser and Bacon 2014)."

Line 71-74 – This is a long sentence. Also should you qualify this statement in view of your paragraph above, i.e. state we are now able to at least resolve eddies mostly equatorward of 50-60N/S BUT we don't resolve high latitude eddies or sub mesoscale or associated energy cascade anywhere. Furthermore, results are sensitive to grid scale closure, particularly viscosity, as you state in your eddy kinetic energy section?
In accordance with the Referee's suggestion, text has been added to specify where the 1/16° resolution is not eddy-resolving: "In this context, we developed a global eddying configuration, where eddying means that the numerical simulation is eddy-resolving in most deep ocean regions equatorward of 60°, while it is mostly only eddy-permitting at higher latitude."

Line 88 – As stated above should it be described as a step forward, particularly for mid latitudes where this resolution resolves eddies but 1/4 doesn't?
We do confirm that, as stated in the abstract, GLOB16 configuration represents a step forward in the CMCC global ocean modelling to resolve eddies in the ocean at mid-latitudes. At line 88, we want to emphasise also that this configuration is, for our modelling group, an accomplishment that open the way toward a new, operational short-term ocean forecast system. We did slightly modify the sentence in "…is a foothold that opens the way for the development of a new, operational short-term ocean forecast system…"

Line 123 – what about connection from Marmara Sea to Aegean - Dardanelles Strait is very important for seasonal freshwater input to Northern Aegean.
We did not mention the Dardanelles Strait into the bathymetry description (section 2.2) because no specific modification was applied there. After interpolating GEBCO dataset on the GLOB16 grid, the Dardanelles strait resulted open and 3-grid-point wide in its narrowest area. We reasoned that

additional hand editing was unnecessary in that location. On the other hand, the Bosphorus strait (with a maximum width of ~3.5 km) was close and we had to modify the bathymetry to connect the Marmara Sea and the Black Sea.

Line 127 – Comment only – I believe some 1/12th NEMO configurations use partial slip in Labrador Sea to generate more eddies to help re-stratification after convection?
This comment refers to ORCA12 configuration. We are aware of a set of sensitivity tests performed by the DRAKKAR group to study the impact of lateral boundary condition on the mixed layer depth (MLD) and eddy kinetic energy (EKE) in the Labrador Sea, the Mediterranean Sea and other location where the boundary current dynamics is relevant. Free slip, partial slip and "variable (local partial)" slip were considered. In the Labrador Sea, for example, their results showed that local partial slip helps to increase EKE with its maximum well located between 60-62°N, and also reduce MLD. They suggested that the best choice is a combination of free slip applied everywhere except few limited patches with no-slip. Those locations have to be identified in order to build a sort of mask. We do agree that this approach might help to improve the GLOB16 results in some areas. A set of improvements is already planned for this configuration, some of them already employed. The lateral boundary conditions are for sure on the list.

Line 141 – Comment only – important to note that uncorrected ERAI interim fields, e.g. radiation fields due to cloud errors, will have large errors which would be expected to impact on or even dominate near surface biases.
We do agree with the referee that errors in the atmospheric forcing may largely affect surface biases. A set of corrections can be applied to ECMWF ERAinterim variables to reduce global and regional biases. For example, in developing the DRAKKAR Forcing Set, Brodeau et al. (2014) corrected ERAinterim winds (weaker than QuikSCAT in the inter-tropical band between 40°S and 40°N), modified air temperature and humidity in the polar regions, reduced the shortwave radiation and increased the longwave radiation, and corrected the precipitation field in the western tropical Atlantic and Pacific oceans. How those corrections can improve the forced simulation has been addressed. Nevertheless, we decided not to follow this approach, but rather using some surface restoration (see reply to next point). Our decision may be justified by a number of arguments. Our ocean-modelling group generally uses the uncorrected-ERAinterim atmospheric reanalysis, conducting an analysis of the effect of the quality of the atmospheric forcing on the high-resolution system was beyond the scope of this study, and this GLOB16 simulation has been used as bedrock for the CMCC global ocean forecast system that uses global ECMWF operational system and forecast as it is released. Note that applying corrections to operational analyses/forecasts is rather dangerous, due to possible unexpected changes in quality of the real-time atmospheric forcing.

Line 158 – Why do you need to use SST restoration? This will mask model errors in near surface fields and there is already inherent relaxation back to air temperature in the forcing set?
The SST relaxation is implemented for a twofold reason: to limit the propagation of the atmospheric forcing biases onto the upper ocean and to compare the results with the twin experiment GLOB4 at lower resolution. The value of the relaxation time-scale was set equal to that used in the 1/4° reanalysis and simulation system (Storto et al., 2016; Haid et al. submitted to The Cryosphere).
However, we acknowledge that, due to the SST relaxation, the verification of the sea surface temperature may be misleading and driven by the relaxation dataset and time-scale. Thus, in the revised version of the manuscript, we focused our analysis (in section 3.1) on the subsurface biases.

Storto, A., S. Masina, and A. Navarra (2016), Evaluation of the CMCC eddy-permitting global ocean physical reanalysis system (C-GLORS, 1982–2012) and its assimilation components. Q.J.R. Meteorol. Soc., 142: 738–758. doi: 10.1002/qj.2673

Line 194 – I wonder why you didn't remove the seasonal cycle of MKE from EKE as otherwise the seasonal cycle of flows will be included in EKE estimates?
Line 194 falls within section 2.7 on the "Output and analysis strategy". We assumed the referee's comment is about the calculation of EKE in section 3. As suggested, the seasonal cycle was estimated and then removed from the time series (Plot 1).
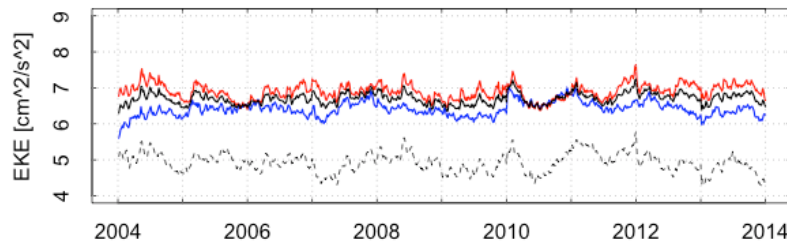
Plot 1. (Fig. 1b in the manuscript) Time variations of volume-averaged EKE (in cm^2 s^{-2}), where the black line represents the global basin-mean value and the red (blue) the contribution of the Southern (Northern) Hemisphere in GLOB16. Thin-dashed line represents the basin-mean EKE in GLOB4.

Line 215 – Can one really say much about SST biases from a ten year run with SST relaxation?
We do agree with the referee. Due to the length of the simulation and the temperature restoring that we applied at the sea surface, the analysis of the SST biases does not add much to our study. We removed the plots showing the surface biases (Fig 2a, b) and accordingly correct the text at the beginning of section 3.1 as follow "The mean fields of modelled potential temperature and salinity are here validated against the mean of EN3 climatology (the UK Met Office Hadley Centre observational dataset, Ingleby and Huddleston 2007), both averaged over the same period 2009-2013. As expected, due to the temperature and salinity restoring applied at the ocean surface, the global mean SST and SSS biases are small (-0.06 for SST and -0.04 for SSS). There are weak cold biases in the tropics, extending over much of the subtropical band, with the largest SST biases (~1 °C warmer) collocated with positive SSS error (0.5–1.5 psu) over the western boundary currents in the Atlantic and North Pacific oceans (not shown). The overall pattern of surface biases is similar between the two models."

Line 215 – Should you show equivalent plots for figs 2 for 1/4 degree or state that they are indistinguishable from the 1/12th if it is? The difference with the 1/4 degree model is surely a key result?
We followed this comment and we added two subplots (e, f) in Figure 2 showing the zonal mean temperature and salinity differences between GLOB4 and observations. Section 3.1 includes now the following text "Although the overall biases are similar between the two model configurations in many latitude bands, there are some relevant differences (Fig. 2e, f). For instance, the Southern Ocean is generally warmer in GLOB4, with a larger positive salinity bias at ~400 m depth around 50°S. Both models are warm and saline in the above depth range in the northern mid and high latitudes, but the biases differ in magnitude and locations, highlighting the difference in path of the western boundary currents. Both models are warmer than observations in the Artic Ocean: the largest warming is confined in the upper 200 m depth in GLOB16, while the maximum, with a similar value, is located between 300 and 500 m depth in GLOB4."

Line 236 – Will the deep (>1000m) ocean really have equilibrated in a ten year run? I am guessing you are probably looking mainly as biases due to isopycnal heave which occurs reasonably fast?

We do agree with the Referee that the integration time required to "spin up" an ocean model from an initial state of rest to a near equilibrium state is much longer for the assessment of the deep ocean. Unfortunately, obtaining equilibrium at eddying resolution is not practical. In 10-year integration, GLOB16 is still in its adjustment phase, especially in the deep ocean. This short simulation is not appropriate for studying the long-term evolution of deep-water masses, as we assert in section 2.6, "The model run for 11 years through the end of 2013, which appears to be a sufficient amount of time for the near-surface velocity field to adjust to the initial density field and for mesoscale processes in the upper ocean to have reached a quasi-equilibrium, while the deep ocean takes much longer to reach steady state." In the paper, we are limited to describe the state of the deep ocean hydrography and overturning circulation after 10 years of integration.

Line 253/296 – More discussion or plots for GLOB4 on figs 3 and 4 would be useful?
Figure 3 includes the time series of AMOC at 26.5°N as reproduced by GLOB4, together with GLOB16 output and RAPID estimates. These results are discussed in section 3.2. We decided not to add plots of the MOC stream functions in the Atlantic, Indo-Pacific and Southern oceans for GLOB4, but we added descriptions of the differences in the overturning circulation between the two configurations for each basin. Both subplots in Figure 4 included GLOB4 results (black lines) as the time-mean Atlantic MHT and its 10-y time series at 26.5°N, also in the previous version of the manuscript. A more detailed description has been added.

Line 263 – Surely one can not say much about AABW in a ten year run?
We do agree that in GLOB16 we cannot evaluate the performances of the model to reproduce the deep ocean circulation in a 10-year run. We limit our purpose to providing estimate of the mean model transport in the bottom layer in such a short simulation.

Line 317 – Implied heat transports assume equilibrium? How large are you heat content tendencies with a short ten year run that may well still be drifting?
One caveat of this study is that the simulations lasted only 10 years.
Comparing actual ocean heat transports with those implied by surface fluxes gives an indication of the volume-averaged drift in temperature. The time evolution of the volume-averaged ocean temperature is shown in Fig 1c to demonstrate the extent to which a quasi-steady state has been reached at the end of the 10-year integration. The potential temperature is seen to decrease by ~0.005°C over 10 years. This drift (related to discrepancies between the actual heat transports by the ocean and the heat transport implied by the surface fluxes) is small enough to assume a close agreement between implied and actual meridional heat transports. That suggests that the GLOB16 ocean is close to quasi-equilibrium.
Then, the time series of the MHT in the Atlantic Ocean at 26°N (at other selected latitudes in the Atlantic Ocean as well – not shown in the paper) does not present any particular trend over the 10-year time window.

Line 430 – I did not think the location of mixed layer maxima agreed so well with the observations in Southern Ocean?
Line 430 is in section 3.3 and concerns the transport in the Mozambique Channel. We think that this comment refers to section 3.4 where locations of mixed layer maxima were mentioned in lines 476-477 (following line numbers in previous section). We deleted this sentence and we kept line 489-490 in which we state that maxima in the Southern Ocean Pacific sector are "not exactly collocated with the observed ones".

Line 430 – How does GLOB4 look in spatial plots? If it is very similar is it worth stating this?
Figure 6 includes now a subplot showing GLOB4 mixed later depth averaged in the Northern (Southern) in March (September) 2009-2013.

6

Line 439 – I wonder if a different temperature based criterion might make the model mixed depths appear better? For example, if there is salinity compensation then density criterion can be rather sensitive to salinity errors.

We applied different criteria to our model output to compute the mixed layer depth. The differences are mainly local and we did not find any general improvement or worsening using different MLD calculations in both hemispheres.

Line 550 – I would emphasize the point about viscosity sensitivity more and include it in introduction. There is often an optimum viscosity level for EKE (and associated MKE) as too little enhances grid scale noise which damps eddies and too much obviously damps eddies.

A clear weakness of this first GLOB16 experiment is its ability in reaching the observed magnitude of EKE, especially in the Southern Ocean. This behaviour is most likely related to the coefficient chosen for lateral momentum diffusion. This GLOB16 simulation suggests that more efforts shall be dedicated to sensitivity experiments for detecting the optimal configuration of horizontal and vertical dynamics. Unfortunately, re-running 10-year experiments is not faceable at the moment. To improve this aspect of GLOB16, we are currently performing short (2year) test experiments.

Line 617 – Southern Ocean MLD maxima appear also not too good in Southern Ocean?

Already answered (please see above the comment to line 430)

Line 633 – As it appears that you change both vertical and spatial resolution it is hard to conclusively attribute GLOB16 versus GLOB4 differences to spatial resolution. Could you state all configuration differences between GLOB4 and GLOB12 configurations as bullet points. In an ideal world one would mimimise the differences, e.g. use same number of vertical levels and vary only viscosity, isopyncal diffusion and perhaps slip between the two runs?

Key differences in parameter settings between the two configurations are now listed in the end of section 2.

Vertical resolution may be adequate for the horizontal scales one is physically concerned with. Lindzen and Fox-Rabinovitz (1989) showed the substantial benefits in refining both horizontal and vertical resolution give some support to scaling arguments deduced from quasi-geostrophic theory implying that horizontal and vertical resolution ought to be chosen consistently. They developed simple physical criteria, based on Rossby radius and gravity wave dispersion, for the vertical resolution consistent with horizontal resolution.

Increasing the vertical resolution in the ocean model can provide a better representation of the upper ocean physics, improve the properties of dense water formation as well as the dynamics of overflow between ocean basins, and more accurately represent the bottom boundary layer physics. The DRAKKAR group showed, for example, improvements in ORCA12 representation of overflows when the vertical levels are changed from 75 to 300.

Both horizontal and vertical resolutions are needed to more accurately depict the 3D structure of the ocean. A multi-step approach to isolate the effects of any specific modification from GLOB4 to GLOB16 was, unfortunately, not viable. Therefore, GLOB16 includes both vertical and horizontal refined grids, and there are no twin runs in which the two configurations do share the same vertical discretization. We attempted to achieve a consistency between horizontal and vertical resolution in our GLOB16 configuration. Applying what we considered to be the most adequate choice (also considering the real limitation due to computational cost), we moved from 75 vertical levels in GLOB4 to 98 in GLOB16, with level spacing from 1 m near the surface to 160 in the deep ocean.

Lindzen, R. S., and M. S. Fox-Rabinovitz, 1989: Consistent vertical and horizontal resolution. Mon. Wea. Rev., 117, 2575– 2583.

We have made the following additional changes to the paper:
In the list of References, we updated Stepanov et al. 2016, Storto et al. 2016.

We corrected the Mozambique Channel transport in Table 2 and accordingly added the following reference
Ridderinkhof, H., P. M. van der Werf, J. E. Ullgren, H. M. van Aken, P. J. van Leeuwen, and W. P. M. de Ruijter: Seasonal and interannual variability in the Mozambique Channel from moored current observations, J. Geophys. Res., 115, C06010, 2010.

Dear Editor and Reviewer,

We would like to thank you for accurately reading and commenting the manuscript, and suggesting how to improve it. Answers to your comments are given in details hereafter. We hope that you will find them satisfactory. All authors agree with the modifications made to the manuscript.
Reviewer comments are in bold, and are followed by our response (in blue) that includes changes and/or additions to the text.

For the authors,
Dorotea Iovino

Answer to **Referee #2**

This manuscript outlines the first results from a new global 1/16° implementation (GLOB16) of the NEMO-LIM ocean-sea ice model. The manuscript outlines some key metrics from the model and compares some metrics to a lower resolution implementations of the same model (GLOB4).
The model described in this manuscript is close to the leading edge of global ocean-sea ice models. It's important to document these models as they develop, and thus there are good reasons for GMD to want to publish this paper. However, there are a number of areas in which the manuscript could be improved.
My primary query is whether this manuscript is here simply to document the existence of a viable model (that is, the model works and is sufficient) or whether the aim is to make the case that the model is an improvement over previous, lower resolution versions. I strongly recommend following the latter path, but I found on reading the paper that the case for the GLOB16 model being an improvement on GLOB4 was somewhat tenuous. For many metrics the GLOB4 results were not shown, and in some areas GLOB4 looked slightly better! If one is to justify the move towards eddy-resolving models then a stronger case that the additional computational expense is worthwhile must be built. (Alternatively, perhaps the conclusion may be that eddy-resolving is not worth the expense until models improve!)

The main objective of this study is to present a new global eddying configuration, to evaluate the first 10-year simulation and, not least, to show the overall improvements of the model solution due to the increasing resolution. For this aim, together with the validation of GLOB16 against observations, we presented a comparison between GLOB16 and the eddy-permitting configuration, GLOB4. As point out by the Referee, this study is certainly enriched by a more detailed analysis of the differences between the two models. We added text and modified plots in any subsection on "model validation" to emphasize the key role played by the ocean resolution.
GLOB16 simulation is by no means perfect, with notable discrepancies with observations in some areas, but we believe that our analysis demonstrates that most aspects of the GLOB16 circulation are more realistic with respect to GLOB4, and the eddying models is able to better represent the upper ocean dynamics and ocean variability at mid- and low latitudes. In particular, our analysis shows that eddying resolution improves the temperature and salinity biases at upper and intermediate depths, the extension and separation of western boundary currents, the strength of the overturning circulation as well as the poleward heat transport in the Atlantic Ocean, the volume transports through most of the considered critical passages, and the narrow boundary currents and flow over narrow sills. Tables 1 and 2 summarize the changes in volume transports.
The biggest caveat of this GLOB16 simulation is the representation of the mesoscale variability. The model has too weak eddy energy compared to observations, and the expected increase in eddy kinetic energy (EKE) due to resolution is not evident. In order to identify the source of this problem, we are analysing this aspect in detail performing a set of short (2-year) sensitivity experiments.

There are more details on these issues in the following list of suggested improvements that the authors may want to consider:

1. The use of acronyms (e.g. NEMO, CMCC) should be avoided in the abstract. In fact, CMCC is never defined in the text of the paper, and it seems unnecessary to list the affiliation of authors within the manuscript.
We deleted the CMCC acronyms in the abstract, substituting it with "Euro-Mediterranean Center on Climate Change". We do think that the acronym NEMO is well known in the ocean modelling community, and as suggested by the editor, we included it in the title and abstract. We deleted the

version of the code that now appears only within the model description in section 2.

2. There is an ambiguous phrase on line 79: ". . . all (most of) the domain. . ." I suggest being more explicit.
We changed the sentence in "… the numerical simulation is eddy-resolving in most deep ocean regions equatorward of 60°, while it is mostly eddy-permitting at higher latitude and over shelf regions."

3. In section 2.3, it's important to list more details about the magnitude of biharmonic viscosity, diffusivity, etc. If it's complicated, then a figure can be justified.
We emphasised the differences in parameter settings between the two configurations at the end of section 2.

4. The SST restoring timescale seems very strong . . . This value needs justification.
The SST relaxation is implemented to limit the propagation of the atmospheric forcing biases into the upper ocean, and thus, with this constrain, reproduce a fairly realistic variability of the upper ocean heat content. The air-sea heat fluxes correction induced by the SST relaxation is shown to drive the strength of deep convection in crucial areas such as Labrador Sea and Nordic Seas, thus also positively impacting the strength of the meridional circulation (Storto et al. 2016).
The value of the relaxation time-scale was set equal to that used in the 1/4° reanalysis and simulation system (Storto et al. 2016; Haid et al. submitted to The Cryosphere) and is chosen as trade-off between the daily frequency of the SST analyses, without strongly constraining the air-sea heat fluxes themselves.
However, we acknowledge that due to the SST relaxation the verification of the sea surface temperature may be misleading and driven by the relaxation dataset and time-scale. Thus, in the revised version of the manuscript we focused our analysis (in section 3.1) on the subsurface biases.

Storto, A., S. Masina, and A. Navarra (2016), Evaluation of the CMCC eddy-permitting global ocean physical reanalysis system (C-GLORS, 1982–2012) and its assimilation components. Q.J.R. Meteorol. Soc., 142: 738–758. doi: 10.1002/qj.2673

Haid, V., D. Iovino, and S. Masina. Impacts of Antarctic runoff changes on the Southern Ocean sea ice in an eddy-permitting sea ice-ocean model. Submitted to The Cryosphere

5. The first part of 2.7 should be shifted to 2.8. It also refers to an appendix which isn't present?
Accordingly to reviewer's suggestions, we removed the text in the subsection 2.7 and moved into subsection 2.8, which has been partially rewritten to highlight the differences between the two configurations and avoid repetition in the set-up description. By mistake, we were still referring to an appendix, initially used to describe the eddy-permitting configuration, and then removed, as suggested by the editor. The descriptions of both models are included in section 2.

6. I don't understand the phrase bi-Laplacian (line 217). I'm used to either Laplacian or biharmonic.
We replaced the word bi-Laplacian by biharmonic.

7. On line 233 and beyond, replace TKE with simply KE (as many fields use TKE to represent Turbulent KE).
Thank you for this comment. We wrongly used the acronym TKE to identify both the Turbulent Kinetic Energy the Total Kinetic Energy. In the revisited version, TKE stays for Turbulent Kinetic Energy in section 2, while "total KE" refers to the total kinetic energy in section 3.

8. In 3.1, I'm not convinced that the mean surface biases mean anything in the presence of such strong restoring.

We do agree with the Referee and we removed the plots showing SST and SSS biases (Fig. 2a and b in previous version). Accordingly, we modified text in section 3.1 as follow "As expected, due to the temperature and salinity restoring applied at surface, the global mean SST and SSS biases are small (-0.06 for SST and -0.04 for SSS). There are weak cold biases in the tropics, extending over much of the subtropical band, with the largest SST biases (over 1 °C) collocated with positive SSS error (0.5–1.5 psu) over the western boundary currents in the Atlantic and North Pacific oceans (not shown)."

9. What is called AIW here is usually referred to as AAIW.

Sorry for this oversight. We corrected the Antarctic Intermediate water acronym in AAIW.

10. I found the results to be somewhat out of order. I suggest putting the global SSH variance maps second, right after the EKE results. In addition, I would put the global transport values before the AMOC results.

We thank the referee for the comment, but we do prefer to keep the actual structure. The global SSH variance is a weakness (probably the largest) of this first GLOB16 experiments. We would prefer not to open the "Model Validation" section with that, but rather to keep it as its close, and recall it in the discussion, where we also suggest how to overcome this weakness.

We liked the idea to move the global MOC before the AMOC, but considering your comments #11, we replaced the global transport computed in depth space with the Southern Ocean MOC computed in density space. After this substitution, it makes sense to us to leave it after Atlantic and Indo-Pacific MOC results.

11. In 3.2, the depth-space overturning means very little in the Southern Ocean. The global MOC should be calculated in density space. The Deacon cell (line 350) is not a physically relevant cell and it would be better to estimate the size of the lower overturning cell in density space.

The use of potential density as the vertical coordinate, rather than depth, is more suitable for representing the MOC in the Southern Ocean, resulting in a better characterization of water mass transport. In particular, the wind-driven Deacon cell, which normally appears in depth-space MOC, is mostly an artefact of zonal and vertical integration at fixed depth level, and does not reflect any real-cross isopycnal flow. Following the Referee's comment, we replaced the global MOC in depth space with the computation in potential density space (where the potential density coordinate is referenced to 2000 db). The new plots for the global density-space MOC is shown below (Plot 1).
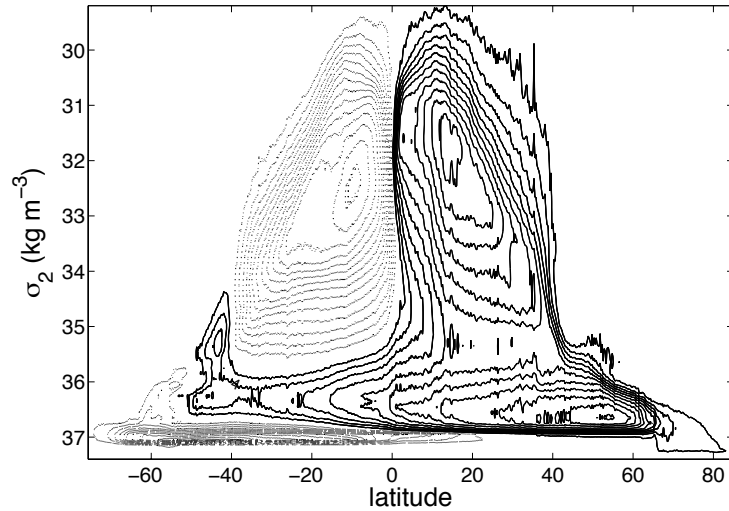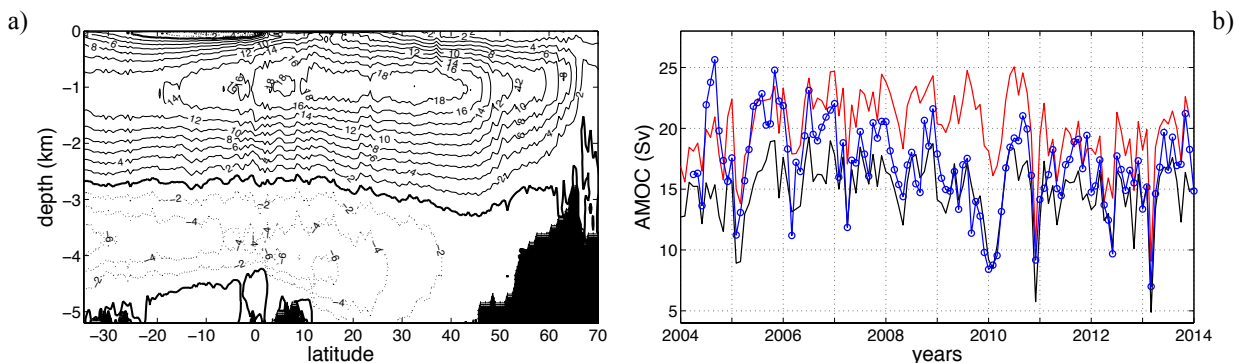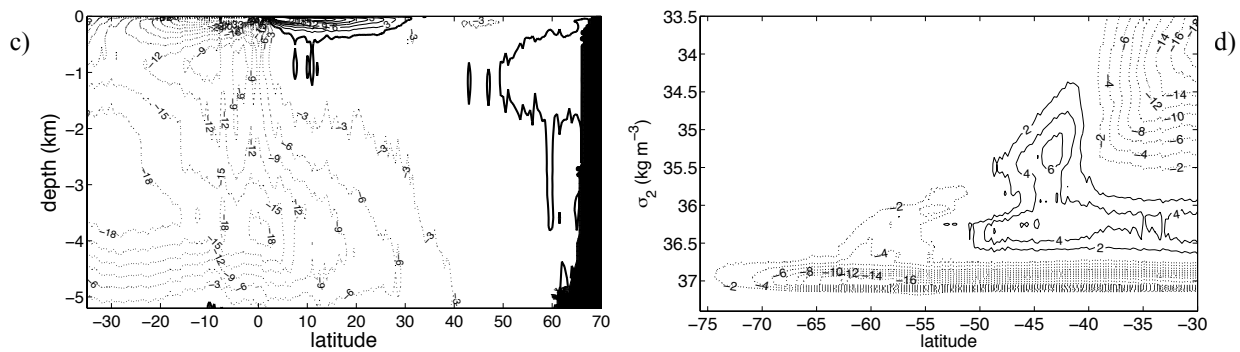
Plot 1. Meridional overturning circulation (in Sv) in potential density space (referenced to 2000 db, σ2) for the global domain. Solid lines represent positive (clockwise) contours. The contour interval is 2 Sv.

In the revisited manuscript, in order to better highlight the Southern Ocean circulation, we display a selected latitude range, from the southernmost boundary to 30ºS.

We added a paragraph to describe the new plot: "The MOC in depth-space is not the most suitable representation of the Southern Ocean overturning circulation. The Deacon cell, for example, is mostly due to a geometrical effect of the east-west slope of the isopycnals and no cross-isopycnal flow is associated with it (Döös and Webb 1994, Farneti et al. 2015). To account for a better characterization of water mass transports, the Southern Ocean MOC is presented in density space as a function of latitude and potential density σ2, referenced to the intermediate depth of 2000 m (Fig. 3d). Three primary cells are identified. The wind-driven subtropical cell is part of the horizontal subtropical gyres and is confined to the lightest density classes. This anticlockwise cell comprises a surface flow spreading poleward to 40S, compensated by an equatorward return flow. GLOB16 produces a subtropical cell of 18 Sv at 32ºS. Below, the upper cell is depicted by the large clockwise circulation, with a time-mean maximum value of 7 Sv. It mainly consists of upper circumpolar deep water that flows at depth southward to ~55ºS, upwells from 36.5 kg m^{-3} to lighter density classes and returns northward as AAIW. The anticlockwise lower cell, in the densest layers, reaches 22 Sv and consists of the poleward lower circumpolar deep water and the deeper equatorward AABW. From 60ºS to the Antarctic continent, the transport represents the contribution of subpolar gyres in the Weddell and Ross Seas. Compared to GLOB16, the Southern Ocean MOC in the eddy-permitting configuration presents a stronger and more extended upper cell, but a slightly weaker transport in the subtropical cell, and an almost absent deep and dense flow in the lower cell (not shown)."

The new Fig 3 is reported below.

5

Plot 2. (Fig. 3 in the manuscript) Meridional overturning stream function (in Sv) averaged over the period 2009–2013, calculated in depth space for (a) the Atlantic and (c) the Indo-Pacific basins, in density space as function of σ_2 for (d) the Southern Ocean. The contour interval is 2 Sv in (a, d) and 3 Sv in (c). Thin solid lines represent positive (clockwise) contours; dashed lines represent negative (anticlockwise) contours. The stream functions were calculated with 0.5º latitudinal spacing to smooth out small-scale variations. (b) Time series of the AMOC at 26.5º N from RAPID observational estimates (blue), GLOB16 (red) and GLOB4 (black) numerical simulations.

12. In Figures 2, 3, 5, 6, 8a,b, 9 and 10 there was no information on the GLOB4 results. However, occasionally, there were references in the text. As noted above, this manuscript will be much stronger if we know where and how improvements between GLOB4 and GLOB16 are manifested, so these results should be included wherever possible.

We thank the referee for this comment. We agree that a more detailed comparison between GLOB16 and GLOB4 can definitely strengthen the manuscript. To present a more complete comparison with GLOB4, we modified subplots and/or add text in any relevant part of section 3, trying not to alter too much the manuscript structure or increase its length.

13. In Fig. 5 I would also like to see a line indicating estimates and errors of each quantity from observations. (Some are listed, some are not). In particular, the Mozambique Channel transport is stated as being "within the range of observed estimates" without a reference!) Also, the ACC transport, listed as the average over all years, is steady and very low for the last 6 years XX it is this equilibrium value that should be listed, not the average over all years.

Thanks for this comment, which helped to improve the plot. On Fig. 5, we added all the observed estimates with associated errors (when available) as reported in Table 2.

To better describe the variability of the ACC transport, we modified the related text in section 3.3 as follow "The zonal circumpolar transport drifts from a mean value of 131.2 Sv in 2004 to 117.3 Sv in 2013. The average volume transport is 122.6 (117.2) Sv over the 2004-2013 (2009-2013) period, lower but comparable to the recent observational estimate over the period 2007-2011 by Chidichimo et al. (2014)." Text describing the Mozambique Channel transport was probably not clear enough. We changed it in "The southward flux across the Mozambique Channel is 23.4 ± 5.4 (20.8 ± 5.8) in GLOB16 (GLOB4) and, for both models, follows within the broad compass of observed estimates, spanning from -29.1 Sv (DiMarco et al. 2002) to -16.7 ± 5.1 Sv (Ridderinkhof et al. 2010)."

14. On line 444, it is ambiguous as to which "two transports are out of phase".

We reworded this sentence as follows "Those transports vary out of phase with each other (Fig. 5d). When the flow is stronger through Fram Strait, it is weaker through Davis Strait and vice versa, indicating that the fluxes out of the Arctic Ocean across those straits partially balance each other."

15. One open question which deserves more investigation is the lack of mesoscale variability in the Southern Ocean. There is a suggestion (in the Conclusion) that this is due to viscous parameterisations, but no quantitative information on what those parameterisations are. The Southern Ocean is one of the key locations where one might expect this resolution to make a

6

dynamical difference, but the very low variability and ACC transport indicate that something is missing here. I suggest a deeper quantitative comparison with other high resolution models is in order.

Yes, the underestimation of Southern Ocean mesoscale variability reproduced in this GLOB16 simulation needed a deeper investigation. Unfortunately, re-running 10-year experiments is not faceable at the moment. To improve this aspect of GLOB16, we are currently performing short (2-year) sensitivity experiments, which includes a set of values of the coefficient for horizontal eddy viscosity. Preliminary results suggest improvements on both the ACC transport and mesoscale variability.

We have made the following additional changes to the paper:
In the list of References, we updated Stepanov et al. 2016, Storto et al. 2016.

We corrected the Mozambique Channel transport in Table 2 and accordingly added the following reference
Ridderinkhof, H., P. M. van der Werf, J. E. Ullgren, H. M. van Aken, P. J. van Leeuwen, and W. P. M. de Ruijter: Seasonal and interannual variability in the Mozambique Channel from moored current observations, J. Geophys. Res., 115, C06010, 2010.

A 1/16° eddying simulation of the global NEMO~~v3.4~~ sea ice-ocean system

Doroteaciro Iovino[1], Simona Masina[1,2], Andrea Storto[1], Andrea Cipollone[1], and Vladimir N. Stepanov[1]

[1]*Fondazione Centro Euro-Mediterraneo sui Cambiamenti Climatici (CMCC), Bologna, Italy*
[2]*Istituto Nazionale di Geofisica e Vulcanologia (INGV), Bologna, Italy*

Abstract

Analysis of a global eddy-resolving simulation using the NEMO ~~(version 3.4)~~ general circulation model is presented. The model has 1/16° horizontal spacing at the equator, employs two displaced poles in the Northern Hemisphere, and uses 98 vertical levels. The simulation was spun up from rest and integrated for 11 model years, using ERA-Interim reanalysis as surface forcing. Primary intent of this hindcast is to test how the model represents upper ocean characteristics and sea ice properties. ~~Numerical results show that, overall, the general circulation is well reproduced, with realistic values for overturning mass and heat transports.~~ Analysis of the zonal averaged temperature and salinity, and the mixed layer depth indicate that the model average state is in good agreement with observed fields and that the model successfully represents the variability in the upper ocean and at intermediate depths. Comparisons against observational estimates of mass transports through key straits indicate that most aspects of the model circulation are realistic. As expected, the simulation exhibits turbulent behaviour and ~~. T~~he spatial distribution of the sea surface height variability from the model is close to the observed pattern. ~~Despite the increase in resolution, the variability amplitude is still weak, in particular in the Southern Ocean.~~ The distribution and volume of the sea ice are, to a large extent, comparable to observed values.

Compared with a corresponding eddy-permitting configuration, the performance of the model is significantly improved: reduced temperature and salinity biases, in particular at intermediate depths; improved mass and heat transports; better representation of fluxes through narrow and shallow straits; increased global-mean eddy kinetic energy (by ~40%). ~~, although r~~ However, ~~R~~relatively minor weaknesses still exist such as, for example, a lower than observed magnitude of the SSH variability. We conclude that the model output is suitable for broader analysis to better understand upper ocean dynamics and ocean variability at global scales. This simulation represents a major step forward in the ~~CMCC~~ global ocean modelling at the Euro-Mediterranean Centre on Climate Change, and constitutes the groundwork for future applications to short-range ocean forecasting.

1. INTRODUCTION

The global ocean is a highly turbulent system over a wide range of space and time scales. Both satellite and in situ data show that mesoscale eddies pervade the ocean at all latitude bands.

Eddies usually account for the peak in the kinetic energy spectrum and most of their energy is generated and maintained by baroclinic instabilities of large-scale flows. Those processes play a substantial role in the dynamics of the global ocean, e.g., transporting and mixing temperature and salinity, exchanging energy and momentum with the mean flow, controlling the mechanisms of deep water spreading and deep convection preconditioning, and modulating air-sea interactions (see e.g. Morrow and Le Traon 2012). The dominant length scale of these eddies varies greatly with latitude, stratification and ocean depth. Mesoscale eddies typically have horizontal scales of the order of the first baroclinic Rossby radius of deformation, varying roughly from 200 km in the tropics to 10-20 km at 50-60° (Chelton et al. 1998), vertical scales ranging from the pycnocline depth to the full ocean depth, and time scales of weeks and months.

Global numerical ocean models, with spatial resolutions ranging from hundred down to a few kilometres, often include both regions where the dominant eddy scales are well resolved and regions where the model resolution is too coarse for eddies to form and hence eddy effects have to be parameterized. In the context of ocean modelling, a model will be eddy rich as long as it uses a horizontal grid mesh whose resolution is fine enough to explicitly (albeit partially) resolve baroclinic and barotropic instability processes, i.e. the grid spacing is finer than the first baroclinic Rossby radius of deformation. Hallberg (2013) showed the model horizontal resolution required to resolve the first baroclinic deformation radius with two grid points, based on a Mercator grid. From his analysis, 1/4° Mercator spacing is insufficient to resolve mesoscale eddies that have a typical scale of 50 km at mid-latitudes. Since the milestone paper by Smith et al. (2000), eddy effects are considered explicitly modelled when the horizontal grids are refined to at least 1/10° (ca. 12 km); however such resolution ~~compares to the Rossby radius and~~ adequately describes both mesoscale variability and western boundary currents only for latitudes lower than ~50°. Resolving mesoscale eddy variability remains anyway elusive at higher latitudes ~~(Hallberg 2013)~~. For example, in the Arctic Ocean where the first Rossby radius decreases down to few kilometres on the continental shelf and in weakly stratified regions, ~~typical eddy-resolving~~ resolution up to about 1/10° does only permit eddies at best (Nurser and Bacon 2014).

~~A key weakness of nearly all global ocean models used to study climate is the absence of an explicit representation of ocean mesoscale eddies, since their spatial scale is smaller than the scale typically resolved by model horizontal grid meshes.~~ ~~Furthermore, o~~Operational oceanography for a variety of different applications such as search-and-rescue, fisheries, and oil spill requires global ocean forecasting systems to reach kilometric scales in coastal areas. This demand is also fostered by the continuous increase of resolution in numerical weather prediction models ~~(Le Traon et al. 2015)~~ and the design of next-generation satellite altimetry missions (Le Traon et al. 2015) that will aim to better capture the ocean mesoscale variability.

These considerations motivate the push toward fully mesoscale eddying ocean models, where the full dynamics and life cycle of baroclinic eddies can be realistically represented over almost the entire global domain. Thanks to progress in ocean modelling and the advances in high performance computing resources over the last decade, ~~oceanic mesoscale eddying~~

numerical simulations at higher resolution are now a realistic choice to bring new insights into the oceanic physical processes ~~operating in the ocean~~ and to find application in ocean ~~Earth system~~ modelling and forecasting. During the last decade, an extensive effort has been made to simulate eddying ocean, different models have been implemented in regional, near-global and fully global domains (e.g. Maltrud and McClean 2005, Chassignet et al. 2009, Oke et al. 2013, Drakkar Group 2014, Metzger et al. 2014, Dupont et al. 2015). In this context, we developed a global eddying configuration, where eddying means that the numerical simulation is eddy-resolving ~~all (most of) the domain~~ in the majority of deep ocean regions, while it is mostly eddy-permitting on the continental shelves or in weakly stratified polar latitudes. Although the increase of resolution does not necessarily lead *per se* to an improved representation of the ocean general circulation, the aim of this work is to evaluate the effect of the explicit solution of eddy dynamics at low- and mid- latitudes on the large-scale dynamics of a high-resolution global ocean model, compared to a coarser resolution configuration. Thus, this manuscript seeks to present the general characteristics of an 11-year spin-up simulation performed with the ocean model configuration, hereunder called GLOB16, at 1/16º (ca. 6.9 km) equatorial resolution, which is performed using the state-of-the-art modelling framework NEMO (Nucleus for European Modelling of the Ocean). The numerical model is a coupled ocean/sea ice model, including a three-dimensional, primitive equation ocean general circulation model and a dynamic-thermodynamic sea ice model. So far, GLOB16 represents the NEMO global configuration having the highest horizontal resolution, and is a foothold that opens the way for ~~the first step in~~ the development of a new, operational short-term ocean forecast system meant to serve as the backbone for downscaling coastal and regional applications to develop services for the global coastal ocean.

The paper is organized as follows. Section 2 describes the model setup, while model analysis is found in Section 3. We rely on comparisons with observations, as well as with a twin eddy-permitting experiment, called GLOB4, as a means of assessing the quality of GLOB16 solution. Conclusions follow in Section 4.

2. MODEL CONFIGURATION

GLOB16 is a global, eddying configuration of the ocean and sea ice system based on version 3.4 of the NEMO ocean model (Madec et al. 2012). The ocean component OPA is a finite difference, hydrostatic, primitive equation ocean general circulation model, with a free sea surface. The ocean component is coupled to the Louvain-la-Neuve sea Ice Model (LIM2) (Fichefet and Maqueda 1997). The ice dynamics are calculated according to external forcing from wind stress, ocean stress and sea surface tilt and internal ice stresses using C grid formulation (Bouillon et al. 2009). The elastic-viscous-plastic (EVP) formulation by Hunke and Dukowicz (1997) is used. The key features of the configuration follow in this section, while a comprehensive technical description of GLOB16 is given in Iovino et al. (2014).

2.1 Mesh

GLOB16 makes use of a non-uniform tripolar grid, computed at CMCC following the semi-analytical method of Madec and Imbard (1996). The horizontal grid has 1/16° resolution at the equator, corresponding to 6.9 km, that increases poleward as cosine of latitude, leading to 5762 x 3963 grid points horizontally. The grid consists of an isotropic Mercator grid from 60°S to 20°N. The meridional scale factor is maintained constant at 3 km south of 60°S. The location of the geographical South Pole is conserved and the domain extents southwards to 78°S, including the ice shelf edge in the Weddell and Ross Seas. North of 20°N, the grid consists of a non-geographic quasi-isotropic grid. To avoid singularities associated with the convergence of meridians at the North Pole, two distinct poles are introduced, whose locations are such that the minimum horizontal resolution is ~2 km around Victoria Island. Ocean and sea ice are on the same horizontal grid. The vertical coordinate system is based on fixed depth levels and consists of 98 vertical levels with a grid spacing increasing from approximately 1 m near the surface to 160 m in the deep ocean.

2.2 Bathymetry

The GLOB16 bathymetry is generated from three distinct topographic products: ETOPO2 (U.S. Department of Commerce 2006) is used for the deep ocean, GEBCO (IOC, IHO and BODC 2003) for the continental shelves shallower than 300 m, and Bedmap2 (Fretwell et al. 2013) for the Antarctic region, ~~from~~ south of 60ºS. The result is modified by two passes of a uniform Shapiro filter, and finally hand editing is performed in key areas. The Black Sea is connected to the Marmara Sea through a 1-grid-point wide channel. The Caspian Sea is all derived from ETOPO2. The maximum depth allowed in the model is 6000 m, the minimum depth is set to 10 m. Bottom topography is represented as partial steps (Barnier et al. 2006).

2.3 Parameterisations

In our simulation, a linearized free surface formulation is used (Roullet and Madec 2000) and a free-slip lateral friction condition is applied at the lateral boundaries. Biharmonic viscosity and diffusivity schemes are used in the horizontal directions in the equations of momentums and tracers, respectively. The values decrease poleward as the cube of the grid cell size. Tracer advection uses a total variance dissipation (TVD) scheme (Zalesak 1979). Vertical mixing is achieved using the TKE turbulent closure scheme (Blanke and Delecluse 1993). Unresolved vertical mixing processes are represented by a background vertical eddy diffusivity of 1.2×10^{-5} m^2 s^{-1}, and a globally constant background viscosity of 1.2×10^{-4} m^2 s^{-1}. Background coefficients of vertical diffusion and viscosity represent the vertical mixing induced by unresolved processes in the model. Vertical eddy mixing of both momentum and tracers is enhanced in case of static instability. The turbulent closure model does not apply any specific modification in ice-covered regions. Bottom friction is quadratic. A diffusion bottom boundary layer parameterization is used for tracers.

2.4 Initialisation

The simulation is started from a state of rest in January 2003, with initial conditions for temperature and salinity derived from the 1995-2004 decade of the World Ocean Atlas 2013 set of climatologies (WOA13; Locarnini et al. 2013, Zweng et al. 2013). The initial conditions for the sea ice (ice concentration, ice thickness) correspond to mean January 2003 produced by a global ocean reanalysis run at 1/4º horizontal resolution (Storto et al. 2016).

2.5 Forcing

Forcing fields are provided from ERA-Interim global atmospheric reanalysis (Dee et al. 2011), released by European Centre for Medium Range Weather Forecasts (ECMWF), with 0.75° spatial resolution. The turbulent variables are 3 hourly and radiative and freshwater fluxes are daily. The surface boundary conditions are prescribed to the model using the bulk formulae proposed by Large and Yeager (2004). The forcing routine and the ice model are called every 4 time-steps (ca. every 13 minutes). A monthly climatology of coastal runoff is derived from Dai and Trenberth (2002) and Dai et al. (2009), with a global annual discharge of ~1.32 Sv (1 Sv = 10^6 m^3 s^{-1}), and is applied along the land mask. The fresh water is added to the surface, assumed to be fresh and at local sea surface temperature. As the thickness of the uppermost level is 0.4 m, diurnal cycle is imposed on solar flux: the daily averaged short wave flux is spread over the day according to time and geographical position (Bernie et al. 2007). The mean sea level is free to drift. Shortwave penetration is applied through the RGB (Red Green Blue) formulation that splits the visible light into three wavebands. The penetration is modulated by a constant chlorophyll value.

2.6 Restoring and spin-up

To avoid drifts in salinity and eventual impacts on the overturning circulation, the sea surface salinity (SSS) is restored toward the monthly objective analyses from the EN4 data set of the Met Office Hadley Centre (Good et al. 2013), with a time scale of 300 days for the upper 50 m. The sea surface temperature (SST) is restored towards the NOAA Optimum Interpolation 1/4° Daily Sea Surface Temperature Analysis (Reynolds et al. 2007) with a constant damping term of 200 W m^{-2} K^{-1}, which corresponds to a restoring time of 12 days. The restoring is identical for the open sea and ice-covered areas. The SST relaxation is implemented to limit the propagation of the atmospheric forcing biases into the upper ocean, and thus, with this constrain, reproduce a fairly realistic variability of the upper ocean heat content. The time step was set to 20 sec for the first 3 days of the simulation, and then increased progressively to reach 200 sec at the 60th day. The model run for 11 years through the end of 2013, which appears to be a sufficient amount of time for the near-surface velocity field to adjust to the initial density field and for mesoscale processes in the upper ocean to have

reached a quasi-equilibrium, while the deep ocean takes much longer to reach steady state. This simulation may be therefore appropriate for studying the dynamics of the ocean circulation on short time scales, but may not for studying the long-term evolution of deep-water masses or climate variability. GLOB16 experiment was performed using 4080 CPU cores on an IBM System x iDataPlex supercomputer. Per simulated year, it required 112000 CPU hours and generated ~3 Tb of output files.

2.7 Output and analysis strategy

~~For comparison purposes, we performed a twin experiment, GLOB4, at eddy-permitting resolution (1/4° at the equator), which is detailed in the Appendix. It employs same numerical schemes and parameterizations as GLOB16, except for the resolution-dependent parameters, such as the horizontal viscosity and diffusivity, sea-ice viscosity, and the time-step length.~~ Model outputs are archived as successive 5-day means throughout the whole integration and post-processed to monthly and annual means. The first simulated year, 2003, is disregarded because of the initial model adjustment; variability in time is analysed over the period 2004-2013, while mean values are computed over the last five years of integrations, from 2009 to 2013, unless otherwise indicated.

2.8 Eddy-permitting configuration

For comparison purposes, we performed a twin experiment, GLOB4, at eddy-permitting resolution, which is also based on version 3.4 of NEMO. This ~~The eddy-permitting GLOB4 is based on version 3.4 of NEMO (Madec et al. 2012). The~~ configuration is a global implementation on an ORCA-like tri-polar grid (Barnier et al. 2006), with a horizontal grid spacing of 0.25° at global scale (1442×1021 grid points). ~~The horizontal grid, known as ORCA025, has 0.25° resolution (1442 grid points × 1021 grid points) at global scale decreasing poleward~~. The effective resolution is ~27.75 km at the equator, and increases as the cosine of latitude with minima of 3.1 km (5.6 km) in the meridional (zonal) direction. The model has 75 vertical levels where the level spacing increases from 1 m near the surface to 200 m at 6000 m. The bathymetry used in GLOB4 is based on the combination of GEBCO in coastal regions and ETOPO2 in open-ocean areas. A uniform Shapiro filter is applied twice, and hand editing is performed in a few key areas. Bottom topography is represented as partial steps.

GLOB4 has sea ice component, atmospheric forcing, bulk formulation and tracer restoring in common with GLOB16. It employs same numerical schemes and parameterizations as GLOB16, except for the resolution-dependent parameters. In particular, the key modifications from GLOB4 to GLOB16 in setting the ocean parameters are a reduction in the biharmonic viscosity from -1.8×10^{11} m^4 s^{-1} to -0.5×10^{9} m^4 s^{-1}; a reduction in the lateral tracer diffusion from 300 m^2 s^{-1} to 80 m^2 s^{-1}; a reduction in the time step from 1080 sec to 200 sec. We do attribute the main differences between the two model configurations to the increase of

ocean resolution, in the horizontal and vertical grid.

~~The model uses a linear free surface and does conserve total energy for general flow and potential enstrophy for horizontally non-divergent flow. The horizontal viscosity is bi-Laplacian with a value of -1.8 × 10¹¹ m⁴ s⁻¹ at the equator, reducing polewards as the cube of the maximum grid cell dimension. Tracers are advected using a total variance dissipation (TVD) formulation. Lateral diffusivity for tracers is parameterized by a Laplacian operator with an eddy diffusivity coefficient of 300 m² s⁻¹ at the equator, decreasing polewards proportionally to the grid size. Vertical diffusion is parameterized by the turbulent kinetic energy (TKE) scheme. Unresolved vertical mixing processes are represented by a background vertical eddy diffusivity of 1.2×10⁻⁵ m² s⁻¹, and a globally constant background viscosity of 1.2 × 10⁻⁴ m² s⁻¹. Bottom friction is quadratic. A diffusive bottom boundary layer scheme is included.~~

3. MODEL VALIDATION

The main objective of this section is to present an overview of the characteristics of the GLOB16 simulation, evaluate its quality against recent observations and highlight the effect of eddying resolution against the eddy-permitting run.

The spin-up of the circulation, as measured by the total kinetic energy (~~T~~KE, defined as $0.5(u^2 + v^2)$ where u and v are the 5-day averages of the horizontal velocity components), potential temperature and salinity averaged over the whole domain, is shown in Fig. 1, and demonstrates the extent to which a quasi-steady state has been reached at the end of the simulation. The total ~~T~~KE of the system increases rapidly during the first simulated year (2003, not shown) and approaches $\sim$12 cm^2 s^{-2} at the beginning of 2004, indicating a baroclinic adjustment of the velocity field to the initial density field. Then, the kinetic energy fluctuates between 11.5 and 12.5 cm^2 s^{-2} for the rest of the simulation, with the highest contribution given by the Southern Ocean (Fig. 1a). Most of the kinetic energy is in the eddy field: the mean GLOB16 eddy kinetic energy (EKE, computed from the 5-day velocity fields using the equation $0.5(u'^2 + v'^2)$, where primes denote deviations from the annual-mean velocities, $(u', v') = (u, v) - (<u>, <v>)$) contributes by $\sim$56% to the total basin-averaged budget (Fig. 1b). As a result of the increased resolution, the time mean of the total ~~T~~KE does not change much over the whole basin (being $\sim$10% larger than in the twin GLOB4 run), while the eddy contribution is boosted by 40% by the eddying resolution.

As expected, in the spin-up stage of the integration, the model adjusts from the WOA13 initial conditions towards the new state imposed by the forcing fields and parameter choices. Both basin-mean potential temperature and salinity show a drift with a clear annual cycle (Fig. 1c,d): temperature decreases by $\sim$0.01 ºC, while salinity presents a small increase of 0.0013 psu over the 10-year period.

3.1 Mean temperature and salinity

The mean fields of modelled potential temperature and salinity are here validated against ~~observations. Figure 2 (a, b) show the SST and SSS biases, relative to~~ the EN3 (the UK Met Office Hadley Centre observational dataset, Ingleby and Huddleston 2007) climatology, both averaged over the same period 2009-2013. As expected, due to the temperature and salinity restoring applied at the ocean surface, the global mean SST and SSS biases are small (-0.06 for SST and -0.04 for SSS). There are weak cold biases in the tropics, extending over much of the subtropical band, with the ~~. The~~ largest SST biases ~~are warm (over~~ (~1 °C warmer)~~, and are~~ collocated with positive SSS error (0.5–1.5 psu) over the western boundary currents in the Atlantic and North Pacific oceans (not shown). The overall pattern of surface biases is similar between the two models. ~~In the Arctic, probably related to biases of air temperature and radiations in the atmospheric forcing (Barnier et al. 2006), there is a positive (negative) surface salinity error of up to 2 psu, where there is an excessive sea ice formation (melting).~~

The surface biases of models forced by prescribed surface boundary conditions are, to a large degree, constrained by the forcing fields, but the analysis of subsurface fields allow for a stronger test of the model, revealing discrepancies in diapycnal mixing and advection pathways. The time- and zonal-average of modelled potential temperature and salinity are shown in Fig. 2 (a~~e~~, b~~d~~), along with their differences from EN3 (Fig. 2c~~2e~~, d~~f~~). GLOB16 temperature field reproduces the expected large-scale features (Fig. 2a~~e~~), with cold waters over all depths at high latitudes and warm water at shallow, low latitudes. GLOB16 salinity also follows expectation (Fig. 2b~~d~~): the low salinity tongue (34.6 psu) of Antarctic Intermediate Water (AAIW), which sinks to ~1500 m depth between 60º-50ºS and propagates toward the equator; an high salinity (up to 35.2 psu) cell centred around 25ºS over the upper 300 m layer; a surface salinity minimum of 34.2 psu at 5º-10ºN connected to the strong precipitation in the inter-tropical convergence zone; high-salinity tongue associated with the Mediterranean Sea at about 35ºN; low-salinity water over the top 200 m north of 45ºN related to the Arctic melt water; and high-salinity (35.2 psu) water below 300 m depth north of 60ºN associated with the formation of cold, dense waters in the North Atlantic. All of these features are clearly present in the observation-based climatology (not shown).

The difference field for temperature (Fig. 2c~~e~~) indicates that the modelled ocean is generally too warm at intermediate depth (100-300 m), with the exception of the AAIW, colder by 0.4 ºC. The largest differences, propagating down to 1000 m, are located in the northern hemisphere from ~40ºN (likely due to the Mediterranean Sea) poleward. The locations of the convective site set the positive and negative biases within the band 60-75ºN. Compared to EN3 temperature, the upper Arctic Ocean in GLOB16 is too warm (up to ~1.4 ºC at ~300 m), mainly due to a warmer Barents Sea inflow. The salinity field reproduced by GLOB16 differs from observations by ~0.15 psu at the most (Fig. 2d~~f~~). Modelled and observed salinities agree well off Antarctica. The model is saltier by 0.1 psu at about 50ºS in the upper 400 m of the water column, and by 0.15 psu at the Equator at ~150 m. The model is too saline (up to 0.1 psu) between 200 and 600 m within the 45-55ºN latitude band, again likely related to the propagation of the Mediterranean overflow in the Atlantic Ocean. Conversely, it is 0.75 psu fresher in the top layer north of 60ºN. The differences between GLOB16 and climatologies for

both fields are small below 1500 m depth. Although the overall biases are similar between the two model configurations in many latitude bands, there are some relevant differences (Fig. 2e, f). For instance, the Southern Ocean is generally warmer in GLOB4, with a larger positive salinity bias at ~400 m depth around 50°S. Both models are warm and saline in the above depth range in the northern mid and high latitudes, but the biases differ in magnitude and locations, highlighting the difference in path of the western boundary current. Both models are warmer than observations in the Arctic Ocean: the largest warming is confined in the upper 200 m depth in GLOB16, while the maximum, with a similar rate, is located between 300 and 500 m depth in GLOB4.

3.2 Volume and heat transports

Transports, in particular the meridional overturning circulation (MOC), are frequently used to evaluate the model performance. To provide an overview of the large-scale general circulation of the GLOB16 model, we present the time-mean meridional overturning stream function of the flow for a zonally averaged view. The MOC ~~displayed in depth space,~~ is shown in Fig. 3, displayed in depth space for the Atlantic and the Indo-Pacific basins, and in density space for the Southern Ocean ~~as well as for the global domain~~. In GLOB16, the Atlantic overturning (AMOC, Fig. 3a) reproduces the two overturning cells linked to the formation of North Atlantic Deep Water (NADW) and Antarctic Bottom Water (AABW). ~~It~~ The upper cell consists of northward surface flow in the top 1000 m, sinking north of 45° (with ~6 Sv sinking north of the Greenland Scotland Ridge), and a southward return flow mainly occurring between depths of ~1000 and ~3000 m. It reaches its maximum strength of ~20 Sv at a depth of 1000 m around 35ºN. An anticlockwise cell, associated with ~~The~~ AABW ~~cell~~, fills the deep ocean below 3000 m, and reaches ~6 Sv. The cross-equatorial transport is ~16.5 Sv. At lower resolution, the overall transport in the Atlantic Ocean is reduced. The transport weakens in both the upper and lower cells, and the NADW flow extents much deeper as it flows southward, reaching ~3500 m at the equator (not shown).

Relevant measurements with respect to the mass transport in the Atlantic Ocean and the associated heat transport are provided by the RAPID/MOCHA program (e.g., Cunningham et al. 2007) that makes the net transport across 26.5°N available since spring 2004. Both models are in very good agreement with the RAPID observations at 26.5ºN. The GLOB16 overturning strength and variability, computed at that latitude for the simulated decade, is 20.1 ± 2.9 Sv, which is stronger than, but reasonably consistent with the RAPID estimates of 17.0 ± 3.6 Sv observed between April 2004 to December 2013 (McCarthy et al. 2015) (Table 2). The GLOB16 and RAPID mean values for the 2009-2013 period are 19.3 ± 3.1 and 15.6 ± 3.2, respectively (Table 1). In Fig. 3b, we compare the time series of the strength of the AMOC at 26.5ºN from the eddying model integration and the RAPID estimates. At that latitude, GLOB16 simulation realistically reproduces the AMOC temporal variability on seasonal and inter-annual time scales, although the simulated variability is lower than the observed. The high-resolution model misrepresents the two events of low AMOC observed in 2009 and 2010,

1   when GLOB16 transport exhibits a clear, but much weaker than RAPID, decline. Time series
2   from the twin 1/4º simulation is also shown. The Atlantic overturning transport is generally
3   weaker in GLOB4, having a mean magnitude of 14.9 ± 2.6 Sv over the 10 simulated year,
4   ~25% lower than the eddying model. GLOB4 underestimates RAPID values in the first
5   simulated years, closely follows RAPID from 2008, and does better capture the interannual
6   variability and the 2009-10 AMOC reductions. Stepanov et al. (under review) suggested that
7   the source of discrepancy between the two models in simulating the AMOC minima at 26.5ºN
8   might be related to the RAPID methodology used for the calculation, which does not fully take
9   into account the impact of the recirculation of the subtropical gyre on the mid-ocean transport.
10   Coarser resolution models, which cannot resolve processes near the western boundary, produce
11   weaker recirculation cell (e.g., Getzlaff et al. 2005, Roussenov et al. 2008, Zhang 2010).
12   Therefore, in GLOB4, a smaller impact of recirculation and eddies leads to a closer
13   correspondence between the model output and RAPID data. Table 1 shows that the good
14   agreement between GLOB16 and RAPID is true not only for the total AMOC transports, but
15   also for its components (the Florida Current, Ekman and the mid-ocean transports). Details on
16   the decomposition of the AMOC reproduced at 26.5ºN are given in Stepanov et al. (2016 ~~under~~
17   ~~review~~).
18   The Indo-Pacific stream function with its intense equatorial upwelling is shown in Fig. 3c.
19   Apart from the uppermost layers, where Ekman transports dominate, the Indo-Pacific is filled
20   by the AABW cell that reaches its maximum values of ~18 Sv between 3000 and 4000 m
21   depth. As expected, the southward flow outcrops in the Northern Hemisphere consistently with
22   intermediate water formation and penetration of water from the circumpolar area near surface
23   and bottom, sandwiching a southward return flow at intermediate depths. Even though the
24   overall structure of the Indo-Pacific MOC does not differ much between the two models, the
25   different resolution corresponds to a ~30% decrease of the deep overturning (not shown).
26   ~~The global MOC (Fig. 3d) shows the northward flow in the upper ocean, ultimately reaching~~
27   ~~the North Atlantic, the deep waters formed in the north (NADW and the diffusively formed~~
28   ~~Indian Deep Water and Pacific Deep Water) that moves toward the Southern Ocean, where the~~
29   ~~directly wind-driven circulation is represented by a strong Deacon cell that peaks to ~27 Sv at~~
30   ~~~200 m depth around 45ºS.~~ The MOC in depth-space is not the most suitable representation of
31   the Southern Ocean overturning circulation. The Deacon cell, for example, is mostly due to a
32   geometrical effect of the east-west slope of the isopycnals and no cross-isopycnal flow is
33   associated with it (Döös and Webb 1994, Farneti et al. 2015). To account for a better
34   characterization of water mass transports, the Southern Ocean MOC is presented in density
35   space as a function of latitude and potential density σ2, referenced to the intermediate depth of
36   2000 m (Fig. 3d). Three primary cells are identified. The wind-driven subtropical cell is part of
37   the horizontal subtropical gyres and is confined to the lightest density classes. This
38   anticlockwise cell comprises a surface flow spreading poleward to 40ºS, compensated by an
39   equatorward return flow. GLOB16 produces a subtropical cell of 18 Sv at 32ºS. Below, the
40   upper cell is depicted by the large clockwise circulation, with a time-mean maximum value of
41   7 Sv. It mainly consists of upper circumpolar deep water that flows at depth southward to

~55ºS, upwells from 36.5 kg m^{-3} to lighter density classes and returns northward as AAIW. The anticlockwise lower cell, in the densest layers, reaches 22 Sv and consists of the poleward lower circumpolar deep water and the deeper equatorward AABW. From 60ºS to the Antarctic continent, the transport represents the contribution of subpolar gyres in the Weddell and Ross Seas. Compared to GLOB16, the Southern Ocean MOC in the eddy-permitting configuration presents a stronger and more extended upper cell, but a slightly weaker transport in the subtropical cell, and an almost absent deep and dense flow in the lower cell (not shown).

In the North Atlantic, the modelled overturning transport is associated with about 1 PW (1 PW = 10^{15} W) of northward heat flux. The 5-year mean meridional heat transport (MHT) for the Atlantic Ocean simulated by GLOB16 is presented in Fig. 4a; transports from GLOB4 and observational estimates are shown for comparison. It is worth noting that the heat transport magnitude and the location of its maximum are data dependent, although the latitudinal variation is comparable among them. The variation with latitude of the ~~GLOB16~~ transport realistically follows observed profiles in both configurations with positive~~; its~~ magnitude ~~is positive~~ at all latitudes, consistent with heat being carried northward in both hemispheres of the Atlantic Ocean~~, and larger than GLOB4 in most of the basin.~~ GLOB16 generally underestimates the heat transport relative to in situ measurements, as also seen in the COREII coarse-resolution models analysed by Danabasoglu et al. (2014) and in the 1/10º climate model by Griffies et al. (2015). However, our eddying-model MHT lies between implied transport estimates: in particular, it is generally below the transport derived from Large and Yeager (2009), but it is always larger than estimates by Trenberth and Fasullo (2008). The MHT maximum is found at ~22°N by Large and Yeager (2009), and is more widely distributed between 20° and 30° N in the estimates of Trenberth and Fasullo (2008). In GLOB16, the MHT reaches 1.1 PW at ~24°, where observations by Lumpkin and Speer (2007) and Ganachaud and Wunsch (2003) are 1.24 ± 0.25 PW and 1.27 ± 0.15 PW, respectively. GLOB4 MHT lies close to the low estimates by Trenberth and Fasullo (2008), and it is smaller than GLOB16 in most of the basin. The MHT maxima in the two models are collocated in latitude, but the eddy-permitting one presents a ~15% lower peak. In GLOB4, the MHT shows a positive slope between 45ºN and 55ºN, indicating a large gain of heat. It is worth noting that this feature, present in many coarse and eddy-permitting models (e.g. Danabasoglu et al. 2014, Grist et al. 2010), is absent in GLOB16, likely due to a correct path of the simulated North Atlantic Current (Danabasoglu et al. 2014, Treguier et al. 2012), as described in Sect. 3.6. The distinct contributions from the overturning and the gyre circulations to GLOB16 ocean heat transport are also computed (according to Johns et al. 2011) and included in Fig. 4a. The overturning contribution dominates over a large latitude range. This is particularly the case between the Equator and 25°N where the overturning component is within one standard deviation of the mean total heat transport. Poleward, the MOC component drops, while the gyre component increases explaining the large GLOB16 MHT north of 40ºN (in agreement to the eddying climate model results by Griffies et al. 2015). The gyre transport becomes comparable to the overturning contribution at ~45°N, and dominating the Atlantic heat transport from 60°N. Apart from the North Atlantic subpolar gyre, the gyre contribution is

relevant between 10°S and the equator, where the gyre and overturning components contribute about equally to the total heat transport. In the eddy-permitting simulation, the overturning and gyre components follow the GLOB16 ones, but the former departs from GLOB16 between 20 and 40°N, being ~0.2 PW weaker, while the latter decreases north of ~35°N to vanish at ~42°N, and then increase again becoming dominant north of 47°N (not shown). This minimum value partially explains the difference between GLOB16 and GLOB4 MHT at 40-45°N.

At 26.5°N, despite a stronger-than-observed AMOC magnitude, GLOB16 underestimates the Atlantic heat transport estimates all through the 10-year RAPID record (2004-2013). Similar behaviour can be seen in many model studies covering a large range of horizontal resolution (e.g., Maltrud and McClean 2005, Mo and Yu 2012, Haines et al. 2013, Danabasoglu et al. 2014). The simulated MHT is lower by ~10% than mean RAPID value that equals 1.24 PW (McCarthy et al. 2015), but the model output agrees, to a greater extent, with the most recent RAPID estimates, which show a decrease of MHT since 2009: the 5-year means of 1.31 ± 0.27 PW for the pentad 2004-2008 drops by 15% to 1.14 ± 0.08 PW for the pentad 2009-2013. The variation in time of the modelled and observed MHT at 26.5ºN is presented in Fig. 4b. Both runs misrepresent the large summer fluxes in the first 2 years of integration. Afterwards, GLOB16 matches very closely the RAPID magnitude and its variability from 2006 on. The eddy-permitting GLOB4, instead, underestimates both the eddying configuration and the RAPID record with a mean value and variability of 0.87 ± 0.21 PW.

3.3 Volume transports through critical sections

Although the two models do generally reproduce similar large-scale ocean circulation, performing high-resolution simulations alters strength, shape and position of the main gyres (Lévy et al. 2010), but especially results in a more accurate representation of narrow boundary currents. To judge the level of agreement between the model velocity fields and the observational data, we list, in Table 2, the time-mean volume transports through well-defined critical straits and passages, evaluated from GLOB16 velocities averaged over the 10 years of integrations, together with GLOB4 values, observation-based estimates and their sources for each region. It is worth noting that the observational products are based on numbers of assumptions and do not always cover the simulated decade.

The strengths of the GLOB16 transports agree well with observations, and are generally within or very close to the limits of observed uncertainty. First, we consider the Drake Passage transport as representative of the large-scale features of the Antarctic Circumpolar Current (ACC). The zonal circumpolar transport drifts from a mean value of 131.2 Sv in 2004 to 117.3 Sv in 2013. The average volume transport is 122.6 (117.2) Sv over the 2004-2013 (2009-2013) period, lower but ~~ranges between about 112 Sv and 137 Sv, with a mean value of 122.6 Sv,~~ comparable to the recent observational estimate over the period 2007-2011 by Chidichimo et al. (2014) ~~and close to the lower bound of the canonical ACC transport from Cunningham et al. (2003)~~. The time-series of the monthly averaged transport, in Fig. 5a, shows a decline of ~10 Sv in the first 3 simulated years, then the drift becomes negligible. As shown by Farneti et al.

1   (2015), at coarser resolution, the mean transport is generally larger than observational

2   estimates. The increase in resolution largely improves the mean ACC transport, which is ~20%

3   stronger in GLOB4.

4   The total Indonesian throughflow (ITF) volume transport estimates from the 3-year INSTANT

5   Program corresponds to 15.0 Sv, varying from 10.7 to 18.7 Sv (Sprintall et al. 2009). The mean

6   ITF transport from GLOB16 (computed at 114ºE, between Indonesia and Australia) falls

7   within this range, but slightly overestimates the observed mean value. The GLOB16

8   contributions to the Pacific-to-Indian Ocean flow across Lombok, Ombai and Timor straits

9   follow within the range of minimum and maximum values from INSTANT (Sprintall et al.

10   2009, Gordon et al. 2010). Beside a weak decrease in the first years of simulation, the ITF has

11   no evident drift over time (Fig. 5b). In GLOB4, the total mean value is closer to observations,

12   but its decomposition is not: the Lombok Strait is closed and is likely compensated by a too

13   strong transport through the Ombai strait.

14   The southward flux across the Mozambique Channel is 23.4 ± 5.4 (20.8 ± 5.8) Sv in GLOB16

15   (GLOB4) and, ~~simulated by~~ for both models, follows within the broad range of observed

16   estimates, spanning from -29.1 Sv (DiMarco et al. 2002) to -16.7 ± 3.1 Sv (Ridderinkhof et al.

17   2010). GLOB16 time series, in Fig. 5c, is characterized by a large seasonal cycle and is free

18   from any significant drift.

19   Comparing the strength of the modelled and observation-based volume transports through the

20   main Arctic Ocean gateways shows that GLOB16 calculations lie within the observed mean

21   values and within the uncertainty range of observations in these areas. The simulated Pacific

22   inflow across the Bering Strait of 1.1 Sv is consistent with observed values in both models,

23   overestimating the recent estimates by Woodgate et al. (2012) to a small degree. The large

24   transport at Bering Strait is common to other NEMO simulations, also at high-resolution (e.g.

25   Marzocchi et al. 2015). For the average outflow from the Arctic Ocean (computed across Fram

26   and Davis straits), the simulated 4.6 Sv are indistinguishable from observations, reproducing a

27   correct partitioning of the exports west and east of Greenland. 2.4 Sv flow southward across

28   the Fram Strait, compared with an observational estimates of 2 ± 2.7 Sv (Schauer et al. 2008),

29   and 2.2 Sv in the Davis Strait against estimates of 2.6 ± 1 Sv (Cuny et al. 2005) and more

30   recent 1.6 ± 0.5 Sv (Curry et al. 2014). Those transports vary out of phase with each other (Fig.

31   5d). When the flow is stronger through Fram Strait, it is weaker through Davis Strait and vice

32   versa, ~~The seasonal cycles of the two transports are out of phase,~~ indicating that the fluxes out

33   of the Arctic Ocean across those straits partially balance each other ~~(Fig. 5d)~~. In contrast,

34   GLOB4 reproduces a stronger transport through the Canadian Archipelago, and underestimates

35   the Fram Strait component.

36   The dense and cold overflows from the Nordic Seas supply the densest waters to NADW (e.g.

37   Eldevik et al. 2009) and have a fundamental impact on the circulation in the Irminger and

38   Labrador Seas, which are active sites of deep-water formation (e.g. Dickson et al. 2008). To

39   assess whether GLOB16 is capable to reproduce the strength of the overflow (here defined as

40    $\sigma_\theta > 27.8$ kg m^{-3}), the corresponding volume transport has been calculated both in the Denmark

41   Strait and in the Faroe Bank Channel. The mean transport appears to be consistent with

observations in the Denmark Strait, with a mean overflow transport of 2.7 Sv across the Denmark Strait, which slightly underestimates the long-term observed transport of ~3 Sv (Macrander et al. 2007, Jochumsen et al. 2012). There is no clear seasonal cycle, and no discernible trend is detected for the whole period (Fig. 5e), as observed by Dickson et al. (2008). The mean transport of dense water across the Faroe Bank Channel is 1.7 Sv with absent trend (Fig. 5e), in well accordance with the observed values of ~2 Sv (Hansen and Østerhus 2007). This consistency builds confidence that the dense water transport processes are realistically simulated in GLOB16. At lower resolution, water-masses at the sill depth in the Denmark Strait are too light compared with observations, resulting in a weak overflow in the considered density class; while the Faroe Bank Channel overflow is too dense, with a consequent large transport.

3.4 Mixed layer depth

Here we evaluate the winter mixed layer depth (MLD) in both hemispheres. MLDs are computed using a density threshold of 0.03 kg m^{-3} from the near-surface value. The two models represent the mixed layer quite realistically, across the global domain, with similar spatial distribution. Figure 6 shows the ~~GLOB16~~ MLD reproduced by GLOB16 and GLOB4 for March (September) in the Northern (Southern) Hemisphere calculated for years 2009-2013, alongside the reconstructed climatology of de Boyer Montégut et al. (2004) for the 1994-2002 period. In general, GLOB16 realistically reproduces the expected spatial patterns of the winter surface mixing, with good correspondence between regions of shallow and deep mixed layers. The model reproduces regions of shallow MLDs in the tropics. ~~Locations of maxima are realistic both in the northern and the southern hemispheres.~~ In the North Atlantic, the sites of winter dense-water formation are realistically located in the subpolar gyre, with the deepest mixing occurring in the Labrador Sea, where it reaches over 2000 m (Fig. 7). In the Nordic Seas, the winter mixing is strong along the path of transformation of Atlantic water in the Norwegian Sea and convective site are reproduced south of Svalbard and in the Iceland Sea with MLDs down to 400 and 1000 m depth, respectively. In the Northern Hemisphere, both runs reproduce mixed layer maxima deeper than observed estimates, as generally seen in NEMO calculations at different resolutions (e.g. Megann et al. 2014, Marzocchi et al. 2015). In GLOB4, the winter mixing in the Nordic Seas is comparable to GLOB16 results, while in the Labrador Sea is shallower than GLOB16 (Fig. 7), but covering a much wider area (~~not shown~~ Fig. 6). In the austral hemisphere, the deepest winter mixed layer corresponds to the near-zonal bands of deep turbulent mixing along the path of the ACC, where the mixed layer deepens in many instances (Sallée et al. 2010). Maximum values of ~800 m are found in the Pacific basin, not exactly collocated with the observed ones (Fig. 6). Both models have a significant deeper mixed layer in regions of AABW formation, associated with densification of the water masses over the Antarctic continental shelf, a result similarly shown in a recent COREII study assessing 15 ocean-sea ice models (Downes et al. 2015). The GLOB16 mixed layer reaches depths of 500 m and 400 m over the Ross Sea and the Weddell Sea continental shelves,

respectively. The time-mean MLD in the Southern Ocean reproduced by GLOB4 is generally shallower than GLOB16 and observations (Fig. 6), but presents deepest maxima close to the Antarctic coast, ~~GLOB4 mixed layer is deeper in the Southern ocean,~~ reaching to over 4000 m in many instances in the first years of integration (Fig. 7).

3.5 Sea ice

Formation and melting of sea ice strongly affect the ocean dynamics both locally in polar regions and in the global ocean, through the contribution of high-latitude processes in deep water production. Here we present sea ice properties and their variability for both hemispheres as simulated by the numerical experiments in comparison with satellite observations. The mean fields are computed over the period 2009-2013, excluding the first 5 years of integration in which the sea ice model is far from the equilibrium. Sea ice extent is defined as the area of the ocean with an ice concentration of at least 10%.

In Fig. 8a, the mean seasonal cycle of sea ice extent reproduced by GLOB16 is compared with products from passive microwave satellites SSM/I processed at the National Snow and Ice Data Center (NSIDC, Cavalieri et al. 1996) for both the north and south polar regions. In the Arctic Ocean, the simulated mean extent of 9.5×10^6 km^2 and the amplitude of the seasonal cycle of 10.3×10^6 km^2 are, to a great extent, in good agreement with the observations (10.8×10^6 km^2 and 10.7×10^6 km^2, respectively). Although the mean sea ice extent is smaller than the satellite estimates by ~10% year-round, the GLOB16 results are largely improved in the end of the run, when the sea ice extent seasonal cycle approaches closely the satellite estimates for both minima and maxima. These results suggest that GLOB16 is able to well represent the sea ice thermodynamics processes after 10 years of integrations.

Figure 8b presents the seasonal cycle of Arctic sea ice volume as simulated in GLOB16 and estimated by the data-assimilative model PIOMAS (Pan-Arctic Ice Ocean Modeling and Assimilation System), which compares well with ICESat and CryoSat2 estimates and can be reasonably considered a proxy for reality (Schweiger et al. 2011). From 2009 on, the GLOB16 sea ice volume (14.4×10^3 km^3) matches very closely PIOMAS values (14.5×10^3 km^3), even if the modelled Arctic sea ice is slightly too thick (thin) during the melting (growing) season. The maximum sea ice volume in GLOB16 is anyway overestimated in winter 2011 and 2012 (not shown), following an increase of thickness due to sea ice drift and then mechanical processes. Overall, the sea ice drift in the Arctic Ocean is similar to what is expected. The transpolar drift and the Beaufort gyre circulation patterns are realistically simulated, but ice velocities are generally too high. Nevertheless, the ice area flux of 74.9×10^3 km^2 month^{-1} across Fram Strait in the simulated decade matches very well to estimates of 75.8 based on using Advanced Synthetic Aperture Radar (ASAR) images and passive microwave measurements (Kloster and Sandven 2011), probably compensated by lower thickness (Fig 8c). The Arctic sea ice extent and volume and their variability in time simulated by GLOB4 almost coincide with GLOB16 output, having mean sea ice extent of 9.3 ($10.9) \times 10^6$ km^2 and mean volume of 14.3 ($7.1) \times 10^3$ km^3 in the northern (southern) hemisphere. GLOB4 underestimates the observed ice area

export out of the Arctic Ocean through the Fram strait by ~13%, with a mean value of 66.1 $\times 10^3$ km^2 month^{-1}.

In the Southern Hemisphere, sea ice extent simulated by the two models is again consistent with observations, but GLOB16 (GLOB4) undervalues the total sea ice extent by 1.6 (1.8) $\times 10^6$ km^2. The low maximum in September accelerates the melting process and results in a larger minimum in February (Fig. 8a). At present, no published long-term record of sea ice volume are available for the Southern Hemisphere, making a formal validation of the model skills in simulating sea ice volumes in that region unachievable. We consider recent ICESat laser altimeter observations covering the period 2003-2008 (Kurts and Markus 2012) for a qualitative comparison with model outputs, although uncertainties are still high (Kern and Spreen 2015). Due to the lower minimum sea ice concentration, both models also likely underestimate sea ice thickness and volume in the austral summer, with a possible feedback on the winter sea ice properties. GLOB16 total volume of ice varies substantially over the annual cycle, with a growth of ~14000 km^3 in fall larger than the ~8800 km^3 by ICESat (Fig. 8b).

The sea ice edge and the ice geographical distribution are generally well simulated in GLOB16, particularly in winter. Comparison between the simulated fields of sea ice concentration and the satellite-based estimates averaged over 2009-2013 shows that the GLOB16 sea ice distribution in the end of the growing seasons is realistic in both hemispheres (Fig. 9a,b and 10c,d), although the model simulates a much uniform sea ice concentration around Antarctica (Fig. 10c,d). Summer minima are well reproduced in terms of ice edge, but the regional concentration shows differences from the observations (Fig. 9c,d, and 10a,b). In the Arctic Ocean, the GLOB16 reproduces the maximum ice concentration close to the Canadian archipelago, but the spatial structure is misrepresented over a large area, with too low sea ice concentration in the eastern-central sector. This is likely to be caused by the SST restoring and to a generally too warm Atlantic Water inflow.

The spatial distribution of the sea ice in March is correctly reproduced in the Southern Ocean, with the highest value in the Ross Sea and close to the Antarctic Peninsula in the Weddell Sea, where the area of maximum concentration is anyway smaller than the observed one. The too low ice concentration in the austral summer is constantly simulated from the beginning of the run, and might be related to a too small sea ice concentration used to initialise the simulation.

3.6 Mesoscale variability

To assess the dynamical capacities of the GLOB16 configuration and to evaluate the gain in representing mesoscale variability due to the higher resolution, Fig. 11 show maps of the sea surface height (SSH) variability, represented by the standard deviation plots, from the eddying ocean compared with the eddy-permitting one and altimetry estimates from AVISO product. The spatial structure and intensity of the SSH variability can be used as indicator of strengths and deficiencies of the mean flow. Both models reproduce the major circulation features estimated from satellite measurements. Large values are collocated with the major current systems associated with the Kuroshio Current, the Gulf Stream, the Loop Current in the Gulf

of Mexico, the strong equatorial current system and, in the southern ocean, the Eastern Australian and the Leeuwin currents, the Brazil and Malvinas current system, the Agulhas Current and the Antarctic Circumpolar Current. Although GLOB4 does a credible work of reproducing the general observed spatial pattern, it simulates vast areas of low SSH variability in the ocean interior, which indicates weaker flow instabilities and fewer meanders. GLOB16 shows additional instabilities in the upper ocean with a spatial structure richer in mesoscale features that cover most of the ocean surface, and is more consistent to the observational estimates.

Examination of individual regions can highlight the improvements in GLOB16. In the Northern Hemisphere, the western boundary currents and their extensions are more sharply reproduced at higher resolution. For example, even if the separation point of the Gulf Stream is not largely modified (at ~37°N), its path and areal extent differ largely between configurations. The GLOB16 current turns northwestward around the Grand Banks, instead continuing eastward across the Atlantic (as in GLOB4). Further offshore, the current separates into a southern branch heading toward the Azores Islands and a second branch flowing towards Newfoundland. This feature is not correctly reproduced in the eddy-permitting case, as in many coarser resolution models, leading to a cold and fresh bias in the northwestern subpolar gyre. The separation of the Kuroshio Current occurs at about the same latitude (~36°N) in both models, but the high variability region of the Kuroshio extension extends out to 180ºE in GLOB16 in close agreement with data, while only reaches to 160ºE in GLOB4.

Some characteristic aspects of the global current systems are still misrepresented, also in the eddying run. The performance of GLOB16 in reproducing the observed magnitude of the SSH variability is a clear weakness. In many locations in the Southern Ocean, the GLOB16 map shows a wider and more homogeneous distribution of oceanic eddies, but mesoscale turbulence tends to be organized into a large numbers of small and relatively weak patches. The local variability in the 1/16° simulation becomes comparable to or lower than that in the 1/4° simulation and the altimeter map. This is pronounced within the main body of the ACC where local maxima have not substantially and positively increased with resolution. In the Agulhas region, the model shows a band of high variability along the paths of the Mozambique Current, the East Madagascar Current, and the Agulhas retroflection, but the modelled SSH variability is again much less than the observed one. In the Brazil Malvinas convergence region the SSH variability presents a local minimum at about 55°W, 42°S but does only partially resemble the observed *C*-shape. Modelled magnitude departs significantly from observations also in the East Australian Current.

SSH variance distribution shows strong qualitative similarities to the EKE for the near surface (not shown). In Fig. 12a, we shows the surface EKE, zonally averaged, as calculated from the two simulations and derived from the OSCAR data set (Ocean Surface Current Analyses Real-time, Bonjean and Lagerloef 2002). OSCAR provides estimates of near-surface ocean currents on a 1/3° grid with a 5 day resolution, combining scatterometer and altimeter data. Quantitatively the models differ significantly from the observations, GLOB16 being the closest. However, both models reproduce higher levels of EKE concentrated at the latitude of

the major current system, at the Equator, about 40° N in the Northern Hemisphere and linked to the ACC and the main western boundary currents in the Southern Ocean. The zonal-averaged EKE profiles emphasize that, despite the local defects, the GLOB16 surface levels of energy exceeds GLOB4 everywhere, except in the equatorial band where the westward extension of the Pacific currents is less pronounced. For the higher resolution model, the surface EKE increases by ~20% relative to GLOB4. Since the two models are forced by identical atmospheric fields, the increase in EKE with resolution arises primarily from increased baroclinic and barotropic instability of the mean flow in the high-resolution model, which tends to generate more meanders and eddies. It has been shown that higher level of near surface EKE closer to the one derived from OSCAR can be obtained by assimilating in-situ and altimeter data in a set of eddy-permitting ORCA025 configurations (Masina et al., 2015). In particular, the assimilation of sea level anomaly has been proven to be effective in introducing mesoscale variability (Storto et al., 2015) underestimated by an eddy-permitting configuration similar to the one used in this work. Our results suggest that the increased resolution of GLOB16 is also able to partially recover part of the observed variability. However, GLOB16 value represents only ~60% of the surface EKE estimated from OSCAR. The kinetic energy of the mean flow (MKE) at surface is similar between the models. It increases by 5% in the 1/16° simulation, reaching 94% of the observed MKE (Fig. 12b).

4. CONCLUSIONS

We have introduced a new global eddying-ocean model configuration, GLOB16, developed at CMCC, and presented an overview from an 11-year simulation. GLOB16 is an implementation of version 3.4 of the NEMO model, with horizontal resolution of at least 1/16° everywhere and 98 vertical levels, together with the LIM2 sea ice model on the same grid.

Overall, the model results are quite satisfactory when compared to observations and the gain due to increased resolution is evident when compared to a coarser-resolution version of the model. Analysis of the model zonally-averaged temperature and salinity, MLD, overturning circulation and associated northward heat transport, lead us to conclude that the model average state is realistic, and that the model realistically represents the variability in the upper ocean and at intermediate depths. GLOB16 model configuration showed good skill in simulating exchanges of mass between ocean basins and through key passages. The contributions from the individual straits in the exports from the Arctic Ocean are within the uncertainties of the observational estimates. The seasonal cycles of total ice area and volume are close to satellite observations and the sea ice extent distribution is very well reproduced in both hemispheres, although sea ice concentration and thickness can be further improved together with sea ice drift. The model is able to hindcast the position and strength of the surface circulation. Pathways of western boundary currents are better resolved compared to the eddy permitting run. Comparisons between the SSH variability from the model and from gridded satellite observations indicate that the model variability spatial pattern is acceptable, with local maxima and minima in the same locations as observations. However, a clear weakness of this first

experiment of ~~the~~ GLOB16 model is its ability in reaching the observed magnitude of the SSH variability, especially in the Southern Ocean. This behaviour is most likely related to the coefficients chosen for ~~vertical and lateral~~ eddy diffusivity ~~and viscosity, and detailed numerical studies are planned to improve these aspects.~~ To improve this aspect, short test experiments are currently being performed employing lower values of the lateral eddy momentum diffusivity. ~~, whose p~~Preliminary results show a more energetic Southern Ocean and an SSH variability much closer to satellite estimates. These results also suggest that more efforts shall be dedicated to sensitivity experiments for detecting the optimal configuration of horizontal and vertical dynamics. It is also possible that the relatively coarse resolution (~0.75°) of the ERA-Interim wind forcing may play a partial role on this underestimation, and whether higher-resolution atmospheric products can overcome this feature is to be investigated. In spite of its shortcomings, we think that GLOB16 represents a significant modelling improvement over the previous configurations of the CMCC global ocean/sea ice models at coarser resolutions. As our first step in exploring the behaviour and fidelity of eddying global models, this simulation sets the necessary groundwork for further, more detailed studies. To potentially ameliorate the model realism, we plan, in the near future, to improve physical parameterizations and include physics upgrades either available or under development in NEMO, such as the full non-linear free surface physics, Langmuir turbulence scheme, vertical mixing parameterizations. We expect that these developments will help address some of the shortcomings identified in this study.

The next phase will be to couple GLOB16 to an ocean/sea ice data assimilation system, similar to that described by Storto et al. (2016). Subsequent to that activity, GLOB16 will constitute the base of a global eddying analysis and short-term forecast system, intended to provide boundary conditions for downscaling and forecasting nested models in the world oceans.

Code availability

The NEMO model is freely available under the CeCILL public licence. After registration on the NEMO website (http://www.nemo-ocean.eu/), users can access the code (via Subversion, http://subversion.apache.org/) and run the model, following the procedure described in the "NEMO Quick Start Guide". The revision number of the code used for this study is 4510. The CMCC NEMOv3.4 code includes some additional modifications, applied to the base code. In particular, we modified the North Pole folding condition, introducing a more sophisticated optimization of the north fold algorithm (Epicoco et al. 2014), which leads to an extra increase in model performances (up to 20% time-reduction on the used architecture) without altering any physical process. The algorithm is now available in NEMO version 3.6. Interested readers can contact the authors for more information on the CMCC NEMOv3.4 code.

References

Barnier, B., G. Madec, T. Penduff, J.M. Molines, A.M. Treguier, J. Le Sommer, A. Beckmann, A. Biastoch, C. Boning, J. Dengg, C. Derval, E. Durand, S. Gulev, E. Remy, C. Talandier, S. Theetten, M. Maltrud, J. McClean, and B. De Cuevas: Impact of partial steps and momentum advection schemes in a global ocean circulation model at eddy permitting resolution. Ocean Dynam., 56, 543–567, 2006.

Bernie, D., E. Guilyardi, G. Madec, J. M. Slingo, and S. J. Woolnough: Impact of resolving the diurnal cycle in an ocean–atmosphere GCM. Part 1: a diurnally forced OGCM. Clim. Dynam., 29(6), 575–590, 2007.

Blanke, B., and P. Delecluse: Variability of the tropical Atlantic Ocean simulated by a general circulation model with two different mixed layer physics. J. Phys. Oceanogr., 23, 1363–1388, 1993.

Bonjean, F., and G. S. E. Lagerloef: Diagnostic model and analysis of the surface currents in the tropical Pacific Ocean. J. Phys. Oceanogr., vol. 32, pg. 2938-2954, 2002.

Bouillon, S., M.M. Maqueda, V. Legat, and T. Fichefet: An elastic-viscous-plastic sea ice model formulated on Arakawa B and C grids. Ocean Model., 27, 174–184, 2009.

Cavalieri, D. J., C. L. Parkinson, P. Gloersen, and H. Zwally: Sea Ice Concentrations from Nimbus-7 SMMR and DMSP SSM/I-SSMIS Passive Microwave Data. Boulder, Colorado USA: NASA DAAC at the National Snow and Ice Data Center. 1996, updated yearly. http://nsidc.org/data/nsidc-0051.html.

Chassignet, E.P., H.E. Hurlburt, E.J. Metzger, O.M. Smedstad, J. Cummings, G.R. Halliwell, Bleck, R. Baraille, A.J. Wallcraft, C. Lozano, H.L. Tolman, A. Srinivasan, S. Hankin, P. Cornillon, R. Weisberg, A. Barth, R. He, F. Werner, and J. Wilkin: U.S. GODAE: Global Ocean Prediction with the HYbrid Coordinate Ocean Model (HYCOM). Oceanography, 22(2), 64-75, 2009.

Chelton, D., R. DeSzoeke, M. Schlax, K. El Naggar, and N. Siwertz: Geographical variability of the first baroclinic Rossby radius of deformation. J. Phys. Oceanogr., 28, 433–460, 1998.

Chidichimo, M.P., K.A. Donohue, D.R. Watts, and K.L. Tracey: Baroclinic transport time series of the Antarctic Circumpolar Current measured in Drake Passage. J. Phys. Oceanogr., 44, 1829–1853, 2014.

1 Cunningham, S.A., S.G. Alderson, B.A. King, and M.A. Brandon: Transport and variability of
2 the Antarctic Circumpolar Current in Drake Passage. J. Geophys. Res., 108, 80-84, 2003.
3
4 Cunningham, S.A., T. Kanzow, D. Rayner, M.O. Baringer, W. E. Johns, J. Marotzke, H.R.
5 Longworth, E.M. Grant, J.J.-M. Hirschi, L. M. Beal, C.S. Meinen, and H.L. Bryden: Temporal
6 Variability of the Atlantic Meridional Overturning Circulation at 26.5º N. Science, 317, 935-
7 938, 2007.
8
9 Curry, B., C. Lee, and B. Petrie: Volume, freshwater and heat fluxes through Davis Strait,
10 2004–05. J. Phys. Oceanogr., 41, 429–436, 2011.
11
12 Curry, B., C. M. Lee, B. Petrie, R. E. Moritz, and R. Kwok: Multiyear Volume, Liquid
13 Freshwater, and Sea Ice Transports through Davis Strait, 2004–10. J. Phys. Oceanogr., 44,
14 1244–1266, 2014.
15
16 Dai, A., and K.E. Trenberth: Estimates of freshwater discharge from continents: latitudinal and
17 seasonal variations. Journal of Hydrometeorology, 3, 660-687, 2002.
18
19 Dai, A., T. Qian, K. E. Trenberth, and J. D. Milliman: Changes in continental freshwater
20 discharge from 1948–2004. J. Climate, 22, 2773–2791, 2009.
21
22 Danabasoglu, G., S.G. Yeager, D. Bailey, E. Behrens, M. Bentsen, D. Bi, A. Biastoch, C.
23 Böning, A. Bozec, V.M. Canuto, C. Cassou, E. Chassignet, A.C. Coward, S. Danilov, N.
24 Diansky, H. Drange, R. Farneti, E. Fernandez, P.G. Fogli, G. Forget, Y. Fujii, S.M. Griffies, A.
25 Gusev, P. Heimbach, A. Howard, T. Jung, M. Kelley, W.G. Large, A. Leboissetier, J. Lu, G.
26 Madec, S.J. Marsland, S. Masina, A. Navarra, A.J.G. Nurser, A. Pirani, D. Salas y Mélia, B.L.
27 Samuels, M. Scheinert, D. Sidorenko, A.-M. Treguier, H. Tsujino, P. Uotila, S. Valcke, A.
28 Voldoire, and Q. Wang: North Atlantic simulations in Coordinated Ocean-ice Reference
29 Experiments phase II (CORE-II). Part I: Mean states. Ocean Model., **73**, 76-107, 2014.
30
31 Dee, D. P., S. M. Uppala, A. J. Simmons, P. Berrisford, P. Poli, S. Kobayashi, U. Andrae, M.
32 A. Balmaseda, G. Balsamo, P. Bauer, P. Bechtold, A. C. M. Beljaars, L. van de Berg, J. Bidlot,
33 N. Bormann, C. Delsol, R. Dragani, M. Fuentes, A. J. Geer, L. Haimberger, S. B. Healy, H.
34 Hersbach, E. V. Hólm, L. Isaksen, P. Kållberg, M., Köhler, M. Matricardi, A. P. McNally, B.
35 M. Monge-Sanz, J.-J. Morcrette, B.-K. Park, C. Peubey, P. de Rosnay, C. Tavolato, J.-N.
36 Thépaut, and F. Vitart: The ERA-Interim reanalysis: configuration and performance of the data
37 assimilation system. Quart. J. R. Meteorol. Soc., vol. 137, no. 656, 553–597, 2011.
38
39 Dickson, R. R., S. Dye, S. Jónsson, A. Köhl, A. Macrander, M. Marnela, J. Meincke, S. Olsen,
40 B. Rudels, H. Valdimarsson, and G. Voet: The overflow flux west of Iceland: Variability,
41 origins and forcing. 2008 In: Dickson, R. R., Meincke, J., Rhines, P. (Eds.), Arctic-Subarctic
42 Ocean Fluxes: Defining the role of the northern seas in climate. Springer, Dordrecht, The
43 Netherlands, pp. 443–474.
44
45 Döös, K., and D. J. Webb: The Deacon cell and the other meridional cells of the Southern
46 Ocean. J. Phys. Oceanogr., 24, 429–442, 1994.
47
48 Downes, S.M., R. Farneti, P. Uotila, S.M. Griffies, S.J. Marsland, D. Bailey, E. Behrens, M.
49 Bentsen, D. Bi, A. Biastoch, C. Böning, A. Bozec, V.M. Canuto, E. Chassignet, G.

1 Danabasoglu, S. Danilov, N. Diansky, H. Drange, P.G. Fogli, A. Gusev, A. Howard, M.
2 Kelley, M. Ilicak, T. Jung, M. Kelley, W.G. Large, A. Leboissetier, M. Long, J. Lu, S. Masina,
3 A. Mishra, A. Navarra, A.J.G. Nurser, L. Patara, B.L. Samuels, D. Sidorenko, P. Spence, H.
4 Tsujino, Q. Wang, and S.G. Yeager: An assessment of Southern Ocean water masses and sea
5 ice during 1988–2007 in a suite of interannual CORE-II simulations. Ocean Model., 94, 67-94,
6 2015.
7
8 The Drakkar Group. DRAKKAR: developing high resolution ocean components for European
9 Earth system models. CLIVAR Exchanges, Special Issue on High Resolution Ocean Climate
10 Modelling, 65, Vol 19 No.2, July 2014.
11
12 Dupont, F., S. Higginson, R. Bourdallé-Badie, Y. Lu, F. Roy, G. C. Smith, J.-F. Lemieux, G.
13 Garric, and F. Davidson: A high-resolution ocean and sea-ice modelling system for the Arctic
14 and North Atlantic oceans. Geosci. Model Dev., 8, 1577-1594, 2015.
15
16 Eldevik, T., J. E. Ø. Nilsen, D. Iovino, K.A. Olsson, A.B. Sandø, and H. Drange: Observed
17 sources and variability of Nordic seas overflow. Nature Geoscience 2, 406–410, 2009.
18
19 Epicoco, I., S. Mocavero, and G. Aloisio: Performance Optimization of NEMO Oceanic Model
20 at high resolution. Geophysical Research Abstracts Vol. 16, EGU2014-4468, 2014.
21
22 Farneti, R., S. M. Downes, S. M. Griffies, S. J. Marsland, E. Behrens, M. Bentsen, D. Bi, A.
23 Biastoch, C. Böning, A. Bozec, V. M. Canuto, E. Chassignet, G. Danabasoglu, S. Danilov, N.
24 Diansky, H. Drange, P.G. Fogli, A. Gusev, R. W. Hallberg, A. Howardh, M. Ilicak, T. Jung,
25 M. Kelley, W. G. Large, A. Leboissetier, M. Long, J. Lu, S. Masina, A. Mishra, A. Navarra,
26 A.J.G. Nurser, L. Patara, B. L. Samuels, D. Sidorenko, H. Tsujino, P. Uotila, Q. Wang, and S.
27 G. Yeager: An assessment of Antarctic Circumpolar Current and Southern Ocean meridional
28 overturning circulation during 1958–2007 in a suite of interannual CORE-II simulations.
29 Ocean Model., 93, 84-120, 2015.
30
31 Fichefet, T., and M.A. Morales Maqueda: Sensitivity of a global sea ice model to the treatment
32 of ice thermodynamics and dynamics. J. Geophys. Res., 102, 12609–12646, 1997.
33
34 Fretwell, P., H. D. Pritchard, D. G. Vaughan, J. L. Bamber, N. E. Barrand, R. Bell, C. Bianchi,
35 R. G. Bingham, D. D. Blankenship, G. Casassa, G. Catania, D. Callens, H. Conway, A. J.
36 Cook, H. F. J. Corr, D. Damaske, V. Damm, F. Ferraccioli, R. Forsberg, S. Fujita, P. Gogineni,
37 J. A. Griggs, R. C. A. Hindmarsh, P. Holmlund, J. W. Holt, R. W. Jacobel, A. Jenkins, W.
38 Jokat, T. Jordan, E. C. King, J. Kohler, W. Krabill, M. Riger-Kusk, K. A. Langley, G.
39 Leitchenkov, C. Leuschen, B. P. Luyendyk, K. Matsuoka, Y. Nogi, O. A. Nost, S. V. Popov, E.
40 Rignot, D. M. Rippin, A. Riviera, J. Roberts, N. Ross, M. J. Siegert, A. M. Smith, D.
41 Steinhage, M. Studinger, B. Sun, B. K. Tinto, B. C. Welch, D. A. Young, C. Xiangbin, and A.
42 Zirizzotti: Bedmap2: improved ice bed, surface and thickness datasets for Antarctica. The
43 Cryosphere, 7, 375-393, 2013.
44
45 Ganachaud, A., and C. Wunsch: Large-scale ocean heat and freshwater transport during the
46 World Ocean Circulation Experiment. J. Climate, 16, 696–705, 2003.
47
48 Getzlaff, J., C. Böning, C. Eden, and A. Biastoch: Signal propagation related to the North
49 Atlantic overturning. Geophys. Res. Lett., 32 (9), L09, 602, 2005.

Good, S.A., M.J. Martin, and N.A. Rayner: En4: quality controlled ocean temperature and salinity profiles and monthly objective analyses with uncertainty estimates. Journal of Geophysical Research: Oceans, 118, 6704–6716, 2013.

Gordon, A. L., J. Sprintall, H. M. Van Aken, D. Susanto, S. Wijffels, R. Molcard, A. Ffield, W. Pranowo, and S. Wirasantosa: The Indonesian throughflow during 2004-2006 as observed by the INSTANT program. Dynamics of Atmospheres and Ocean, 50, Issue 2, Pages 115-128, 2010.

Griffies, S. M., M. Winton, W. G. Anderson, R. Benson, T. L. Delworth, C. O. Dufour, J. P. Dunne, P. Goddard, A. K. Morrison, A. T. Wittenberg, J. Yin, and R. Zhang: Impacts on ocean heat from transient mesoscale eddies in a hierarchy of climate models. J. Climate, 28(3), 2015.

Grist, J. P., S.A. Josey, R. Marsh, S.A. Good, A.C. Coward, B.A. de Cuevas, S.G. Alderson, A. New, L. Adrian, and G. Madec: The roles of surface heat flux and ocean heat transport convergence in determining Atlantic Ocean temperature variability. Ocean Dynam., 60, (4), 771-790, 2010.

Haines, K., V.N. Stepanov, M. Valdivieso, and H. Zuo: Atlantic meridional heat transports in two ocean reanalyses evaluated against the RAPID array. Geophys. Res. Lett., 40, 343–348, 2013.

Hallberg, R.: Using a resolution function to regulate parameterizations of oceanic mesoscale eddy effects. Ocean Model., 72, 92–103, 2013.

Hansen, B., and S. Østerhus: Faroe Bank Channel overflow 1995-2005. Progr. Oceanogr., 75, 817–856, 2007.

Hunke, E.C., and J.K. Dukowicz: An elastic–viscous–plastic model for sea ice dynamics an elastic–viscous–plastic model for sea ice dynamics an elastic–viscous– plastic model for sea ice dynamics. J. Phys. Oceanogr., 27, 1849–1867, 1997.

IOC, IHO and BODC: Centenary Edition of the GEBCO Digital Atlas, published on CD-ROM on behalf of the Intergovernmental Oceanographic Commission and the International Hydrographic Organization as part of the General Bathymetric Chart of the Oceans, British Oceanographic Data Centre, Liverpool, U. K., 2003.

Ingleby, B., and M. Huddleston: Quality control of ocean temperature and salinity profiles - Historical and real-time data. J. Marine Syst., 65, 158–175, 2007.

Iovino, D., A. Storto, S. Masina, A. Cipollone, and V. Stepanov: GLOB16, the CMCC global mesoscale-eddying ocean. Research Papers Issue RP0247, December 2014.

Jochumsen, K., D. Quadfasel, H. Valdimarsson, and S. Jónsson: Variability of the Denmark Strait overflow: Moored time series from 1996–2011. J. Geophys. Res., 117, C12003, 2012.

Johns, W. E., M. O. Baringer, L. M. Beal, S. A. Cunningham, T. Kanzow, H. L. Bryden, J. J. M. Hirschi, J. Marotzke, C. S. Meinen, B. Shaw, and R. Curry: Continuous, Array-Based Estimates of Atlantic Ocean Heat Transport at 26.5°N. J. Climate, 24, 2429–2449, 2011.

Kern, S., and G. Spreen: Uncertainties in Antarctic sea-ice thickness retrieval from ICESat. Annals of Glaciology, vol. 56, issue 69, pp. 107-119, 2015.

Kloster K., and S. Sandven: Ice motion and ice area flux in the Fram Strait at 79N using ASAR and passive microwave for Feb. 2004 – Jul. 2010, Tech. Rep. 322, Nansen Environmental and Remote Sensing Center, 2011.

Kurtz, N.T., and T. Markus: Satellite observations of Antarctic sea ice thickness and volume. J. Geophys. Res. 117, C08025, 2012.

Large, W., and S. Yeager: Diurnal to decadal global forcing for ocean sea ice models: the data set and fluxes climatologies, Rep. NCAR/TN-460+STR, National Center for Atmospheric Research, Boulder, Colorado, 2004.

Large, W., and S. Yeager: The global climatology of an interannually varying air-sea flux data set. Clim. Dynam., 33, 341 – 364, 2009.

Le Traon, P.-Y., D. Antoine, A. Bentamy, H. Bonekamp, L.A. Breivik, B. Chapron, G. Corlett, G. Dibarboure, P. DiGiacomo, C. Donlon, Y. Faugère, J. Font, F. GirardArdhuin, F. Gohin, J.A. Johannessen, M. Kamachi, G. Lagerloef, J. Lambin, G. Larnicol, P. Le Borgne, E. Leuliette, E. Lindstrom, M.J. Martin, E. Maturi, L. Miller, L. Mingsen, R. Morrow, N. Reul, M.H. Rio, H. Roquet, R. Santoleri & J. Wilkin: Use of satellite observations for operational oceanography: recent achievements and future prospects. J. Oper. Oceanogr., 8:sup1, s12-s27, 2015.

Lévy, M., P. Klein, A.-M. Tréguier, D. Iovino, G. Madec, S. Masson, and K. Takahashi: Modifications of gyre circulation by sub-mesoscale physics. Ocean Model., 34, 1-15, 2010.

Locarnini, R.A., A.V. Mishonov, J.I. Antonov, T.P. Boyer, H.E. Garcia, O.K. Baranova, M.M. Zweng, C.R. Paver, J.R. Reagan, D.R. Johnson, M. Hamilton, and D. Seidov: World Ocean Atlas 2013, Volume 1: Temperature. S. Levitus, Ed., A. Mishonov Technical Ed.; NOAA Atlas NESDIS 73, 40 pp., 2013.

Lumpkin, R., and K. Speer: Global ocean meridional overturning. J. Phys. Oceanogr., 37, 2550–2562, 2007.

Macrander, A., R.H. Käse, U. Send, H. Valdimarsson, and S. Jónsson: Spatial and temporal structure of the Denmark Strait Overflow revealed by acoustic observations. Ocean. Dyn, 57, 75–89, 2007.

Madec, G. and M. Imbard: A global ocean mesh to overcome the North Pole singularity. Clim. Dynam., 12, 381–388, 1996.

Madec, G. and the NEMO team: Nemo ocean engine - version 3.4. Technical Report ISSN No 1288–1619, Pôle de modélisation de l'Institut Pierre-Simon Laplace No 27, 2012.

Maltrud, M. E., and J. L. McClean: An eddy resolving global 1/10° ocean simulation. Ocean Model., 8, 31–54, 2005.

Marzocchi, A., J. J.-M. Hirschi, N. P. Holliday, S. A. Cunningham, A. T. Blaker, and A. C. Coward: The North Atlantic subpolar circulation in an eddy-resolving global ocean model. J. Marine Syst.,142. 126-143, 2015.

McCarthy, G.D., D.A. Smeed, W.E. Johns, E. Frajka-Williams, B.I. Moat, D. Rayner, M.O. Baringer, C.S. Meinen, J. Collins, and H.L. Bryden: Measuring the Atlantic Meridional Overturning Circulation at 26°N. Prog. Oceanog., 130, 91-111, 2015.

Megann, A., D. Storkey, Y. Aksenov, S. Alderson, D. Calvert, T. Graham, P. Hyder, J. Siddorn, B. Sinha: GO5.0: the joint NERC-Met Office NEMO global ocean model for use in coupled and forced applications. Geosci. Model Dev., 7, 1069–1092, 2014.

Metzger, E.J., O.M. Smedstad, P.G. Thoppil, H.E. Hurlburt, J.A. Cummings, A.J. Wallcraft, L. Zamudio, D.S. Franklin, P.G. Posey, M.W. Phelps, P.J. Hogan, F.L. Bub, and C.J. DeHaan: US Navy operational global ocean and Arctic ice prediction systems. Oceanography 27(3):32–43, 2014.

Mo, H.-E., and Y.-Q. Yu: Simulation of volume and heat transport along 26.5°N in the Atlantic. Atmos. Oceanic Sci. Lett., 5, 373–378, 2012.

Morrow, R., and P.Y. Le Traon: Recent advances in observing mesoscale ocean dynamics with satellite altimetry. Advances in Space Research, 50 (8), 1062–1076, 2012.

Nurser, A.J.G., and S. Bacon: The Rossby radius in the Arctic Ocean. Ocean Science, 10, 967–975, 2014.

Oke, P.R., D.A. Griffin, A. Schiller, R.J. Matear, R. Fiedler, J. Mansbridge, A. Lenton, M. Cahill, M.A. Chamberlain, and K. Ridgway: Evaluation of a near-global eddy-resolving ocean model. Geosci. Model Dev., 6, 591-615, 2013.

Reynolds, R.W., T.M. Smith, C. Liu, D.B. Chelton, K.S. Casey, and M. G. Schlax. Daily high-resolution-blended analyses for sea surface temperature. J. Climate, 20, 5473–5496, 2007.

Ridderinkhof, H., P. M. van der Werf, J. E. Ullgren, H. M. van Aken, P. J. van Leeuwen, and W. P. M. de Ruijter: Seasonal and interannual variability in the Mozambique Channel from moored current observations, J. Geophys. Res., 115, C06010, 2010.

Roullet, G. and G. Madec: salt conservation, free surface, and varying levels: a new formulation for ocean general circulation models. J. Geophys. Res., 105, 23927–23942, 2000.

Roussenov, V., R. Williams, C. Hughes, and R. Bingham: Boundary wave communication of bottom pressure and overturning changes for the North Atlantic. J. Geophys. Res, 113 (C8), C08042, 2008.

Smith, R.D., M.E. Maltrud, F. Bryan, and M.W. Hecht: Numerical simulation of the North Atlantic Ocean at 1/10. J. Phys. Oceanogr., 30, 1532–1561, 2000.

Schweiger, A., R. Lindsay, J. Zhang, M. Steele, and H. Stern: Uncertainty in modeled arctic sea ice volume. J. Geophys. Res., 116, C00D06, 2011.

Sprintall, J., S. E. Wijffels, R. Molcard, and I. Jaya: Direct estimates of the Indonesian Throughflow entering the Indian Ocean: 2004–2006. J. Geophys. Res., 114, C07001, 2009.

Stepanov, V. N., D. Iovino, S. Masina, A. Storto, and A. Cipollone: Methods of calculation of the Atlantic meridional heat and volume transports from ocean models at 26.5°N. J. Geophys. Res. Oceans, 121, 1459–1475, 2016. *Under review to Journal of Geophysical Research: Oceans.*

Storto A., S. Masina and A. Navarra: Evaluation of the CMCC eddy-permitting global ocean physical reanalysis system (C-GLORS, 1982-2012) and its assimilation components. Quart. J. R. Meteorol. Soc., 142, 738–758, 2016. doi: 10.1002/qj.2673, 2015.

Treguier, A.M., J. Deshayes, C. Lique, R. Dussin, J.M. Molines: Eddy contributions to the meridional transport of salt in the North Atlantic. J. Geophys. Res., 117 (C5), 2012.

Trenberth, K. E., and J. T. Fasullo: An observational estimate of inferred ocean energy divergence. J. Climate, 38, 984–999, 2008.

Woodgate, R. A., T. J. Weingartner, and R. Lindsay: Observed increases in Bering Strait oceanic fluxes from the Pacific to the Arctic from 2001 to 2011 and their impacts on the Arctic Ocean water column, Geophys. Res. Lett., 39, L24603, 2012.

Zalesak, S. T.: Fully multidimensional flux corrected transport for fluids. J. Comput. Phys., 31, 335–362, 1979.

Zhang, R.: Latitudinal dependence of Atlantic meridional overturning circulation (AMOC) variations. Geophys. Res. Lett., 37, L16703, 2010.

Zweng, M.M., J.R. Reagan, J.I. Antonov, R.A. Locarnini, A.V. Mishonov, T.P. Boyer, H.E. Garcia, O.K. Baranova, D.R. Johnson, D. Seidov, and M.M. Biddle. World Ocean Atlas 2013, Volume 2: Salinity. S. Levitus, Ed., A. Mishonov Technical Ed.; NOAA Atlas NESDIS 74, 39 pp., 2013.

Table 1. AMOC and its constituents with standard deviations, averaged within the 2009-2013 period as obtained from RAPID observations and the two models at 26.5ºN. The modelled Gulf Stream transports include both the Florida current and Western boundary current contributions.

	RAPID	GLOB16	GLOB4
AMOC	15.6 ± 3.2	19.3 ± 3.1	14.3 ± 2.7
Ekman	3.3 ± 2.3	2.7 ± 2.4	2.7 ± 2.3
Gulf stream	31.2 ± 2.3	34.9 ± 2.7	32.2 ± 2.1
Upper Mid-Ocean	-18.9 ± 2.8	-19.8 ± 2.0	-21.3 ± 1.6
Throughflow	0	-1.6 ± 0.5	-0.8 ± 0.5

Table 2. Volume transports (in Sv) through key sections, simulated values averaged in the 2004-2013 period and observed mean values with their standard deviations (when available). Positive values correspond to northward and eastward flows.

|	GLOB16	OBSERVED		GLOB4
max AMOC at 26.5°N	20.1 ± 2.9	17 ± 3.6	McCarthy et al. 2015	14.9 ± 2.6
Drake Passage	122.6 ± 5.7	~~136.7 ± 6.9~~	~~Cunningham et al. 2003~~	149.5 ± 9.5
		127.7 ± 8.1	Chidichimo et al. 2014	
ITF (total at 114°E)	-18.1 ± 2.5	-15 ± 4	Sprintall et al. 2009	-16.1 ± 2.8
Lombok Strait	-2.2 ± 1.9	-1.8 to -3.2	Sprintall et al. 2009	--------
		-2.6	Gordon et al. 2010	
Ombai Strait	-4.7 ± 2.2	-2.7 to -5.0	Sprintall et al. 2009	-5.7 ± 1.4
		-4.9	Gordon et al. 2010	
Timor Passage	-6.8 ± 1.8	-6.2 to -10.5	Sprintall et al. 2009	-7.2 ± 1.6
		-7.5	Gordon et al. 2010	
Mozambique Channel	-23.4 ± 5.4	-29.1	DiMarco et al. 2002	-20.8 ± 5.8
		-16.7 ± 3.1	Ridderinkhof ~~van der Werf~~ et al. 2010	
Bering Strait	1.1 ± 0.5	0.8 ± 0.2	Woodgate et al. 2012	1.1 ± 0.5
Fram Strait	-2.4 ± 1.0	-2.0 ± 2.7	Schauer et al. 2008	-1.5 ± 1.2
		-2.3 ± 4.3	Curry et al. 2011	
Davis Strait	-2.2 ± 0.5	-2.6 ± 1.0	Cuny et al. 2005	-3.4 ± 0.9
		-1.6 ± 0.5	Curry et al. 2014	
Denmark Strait overflow	-2.7 ± 0.4	-3.4 ± 1.4	Jochumsen et al. 2012	-1.4 ± 0.3
FBC overflow	-1.7 ± 0.2	-1.9 ± 0.3	Hansen and Østerhus 2007	-2.5 ± 0.3
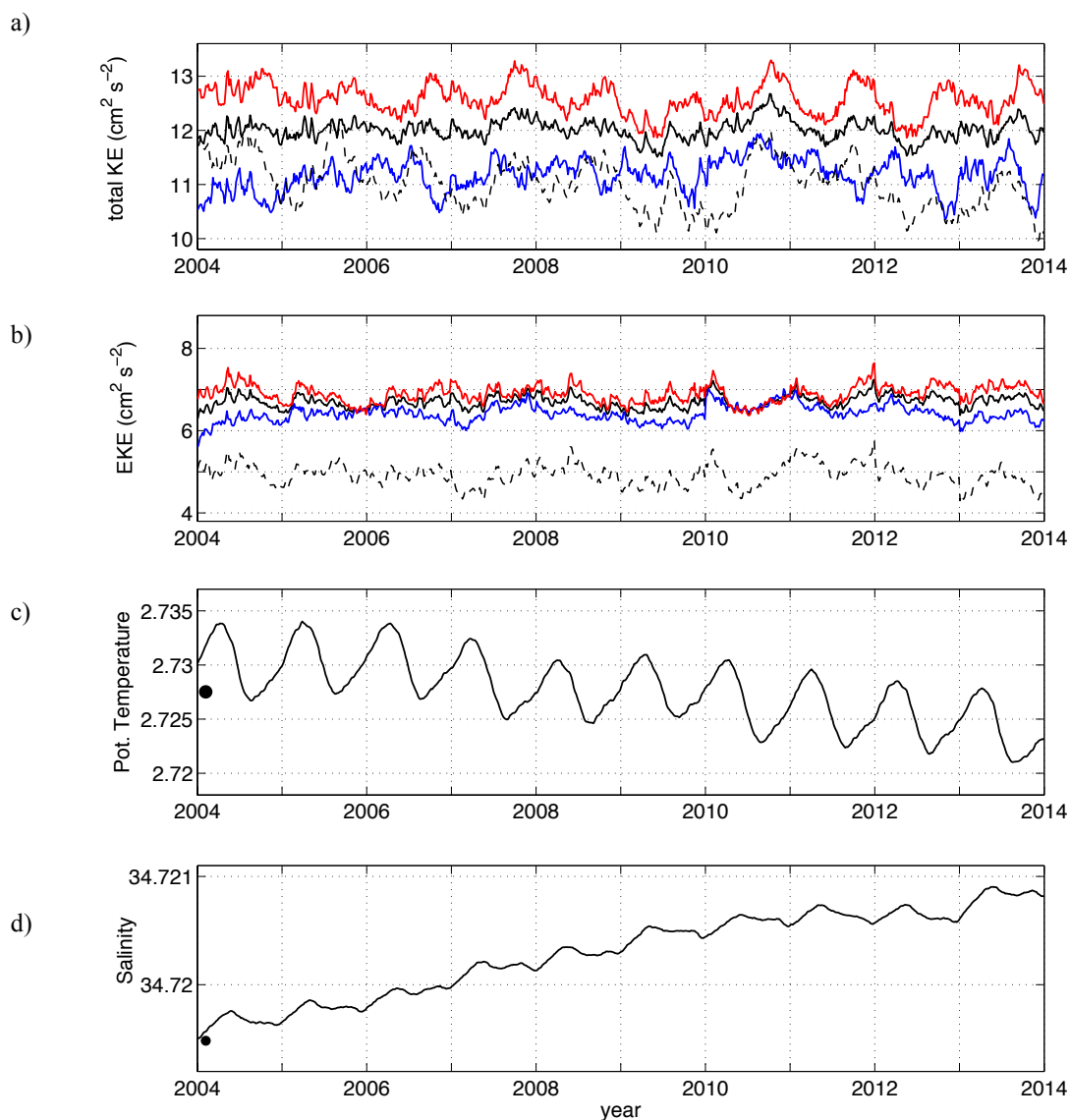
Fig. 1. Time variations of volume-averaged (a) total TKE (in cm^2 s^{-2}), where the black line represents the global basin-mean value and the red (blue) the contribution of the Southern (Northern) Hemisphere in GLOB16. Thin-dashed line represents the basin-mean total TKE in GLOB4. (b) As (a) but for EKE (in cm^2 s^{-2}). The seasonal cycle of the mean field has been removed. (c) Potential temperature in °C, and (d) salinity in psu. Black circles indicate temperature and salinity initial values.
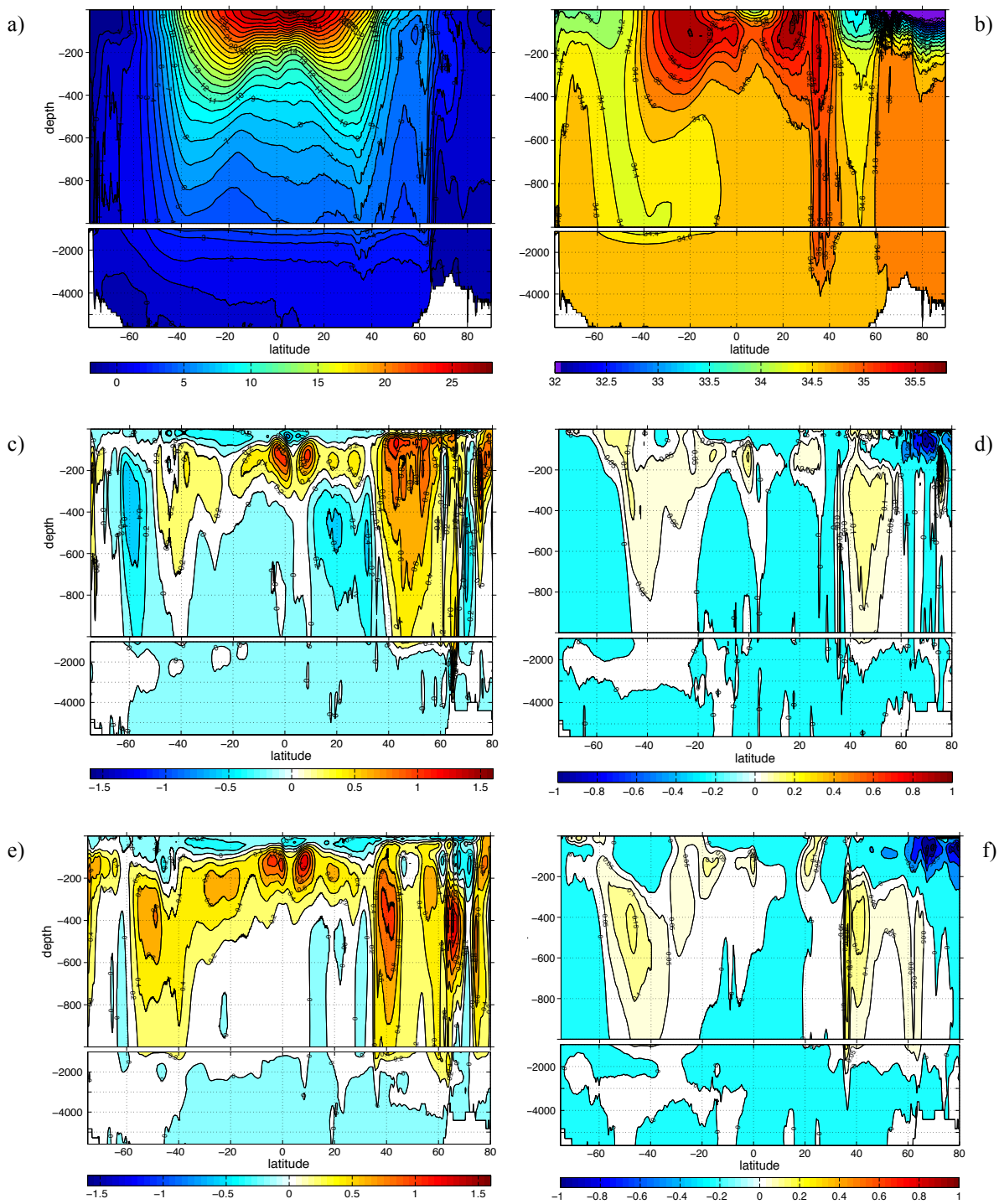
Fig. 2. (a, b) GLOB16 ~~surface biases in years 2009-2013 for temperature and salinity. (c, d) Modelled~~ zonal mean temperature (left column) and salinity (right column) in years 2009-2013 and (~~c~~e, ~~f~~d) differences with EN3 dataset. (e, f) As (c, d), but for GLOB4. Black and Caspian Sea are not considered in the zonal mean. ~~Temperature (salinity) is in the left (right) column.~~ The contour interval is 1 ℃ in (a), 0.2 ℃ in (~~a~~c, e), ~~1 ℃ in (b), 0.05 psu in (b,f),~~ 0.2 psu in (~~d~~b), 0.05 psu in (d, f). ~~In (a,b) model output and observations are shown on the eddy permitting ORCA grid. Numbers of grid points are indicated on the axis, along with indications of latitudes and longitudes.~~
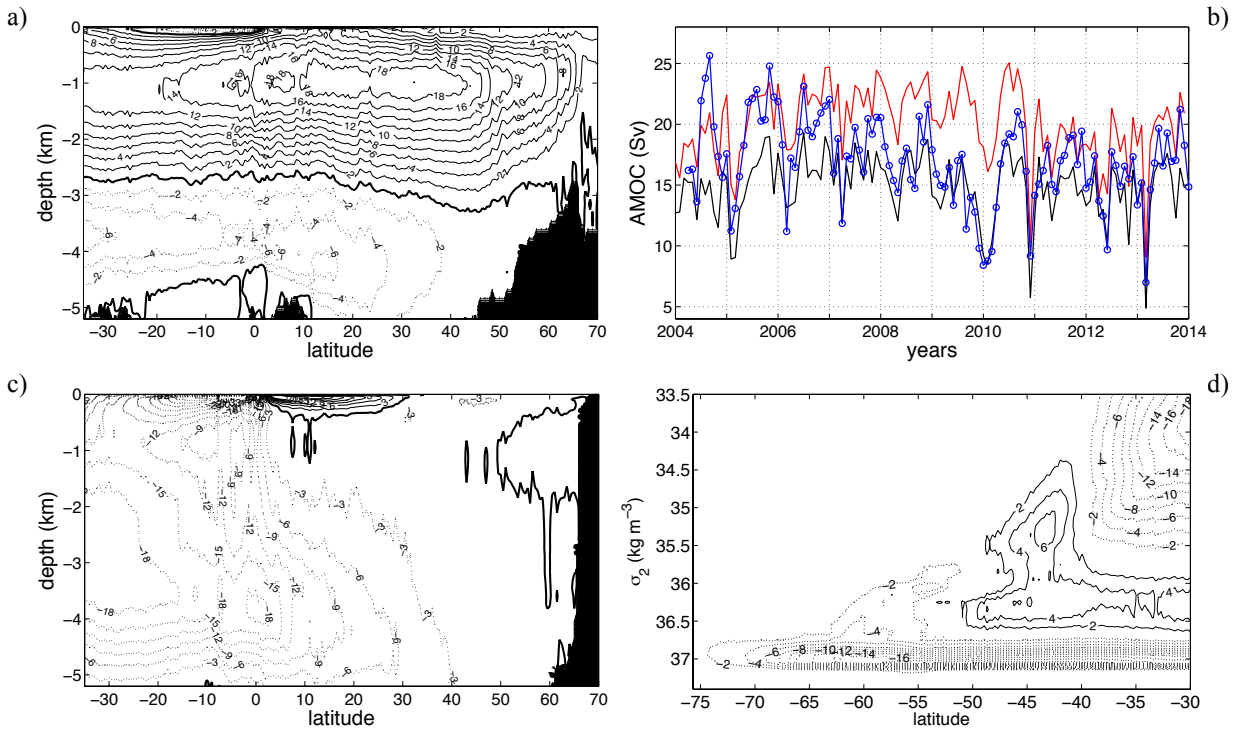
Fig. 3. Meridional overturning stream function (in Sv) averaged over the period 2009–2013, calculated in depth space for (a) the Atlantic and (c) the Indo-Pacific basins, and in density space as function of σ_2 for (d) the Southern Ocean. The contour interval is 2 Sv in (a, d) and 3 Sv in (c). Thin solid lines represent positive (clockwise) contours; thick solid lines represent zero contours. The stream functions were calculated with 0.5° latitudinal spacing to smooth out small-scale variations. (b) Time series of the AMOC at 26.5° N from RAPID observational estimates (blue), GLOB16 (red) and GLOB4 (black) numerical simulations.
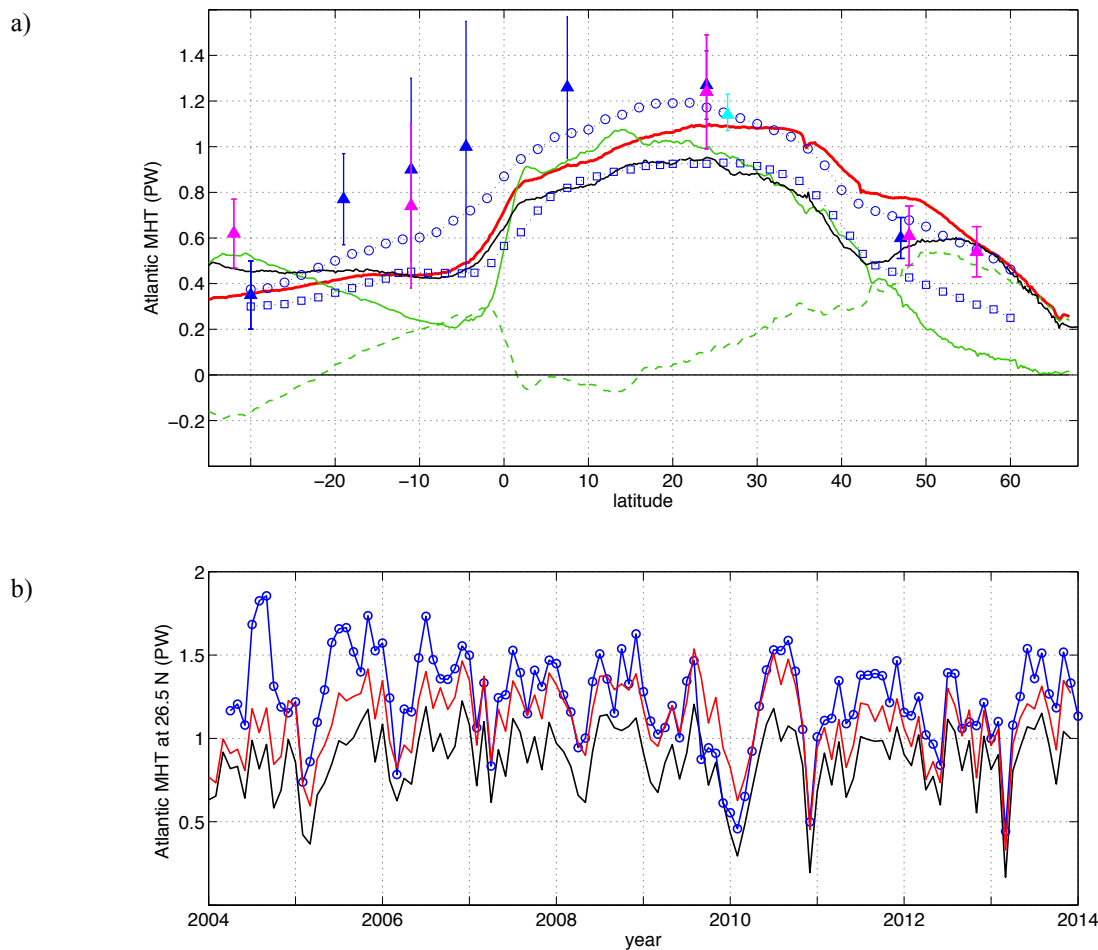
Fig. 4. (a) Time-mean Atlantic MHT (in PW) as a function of latitude. Red line is the total GLOB16 transport with its overturning (green) and gyre (dashed green) ~~and~~ components. Black line represents the total GLOB4 transport. Blue circles (squares) represent implied time-mean transport calculated by Large and Yeager 2009 (Trenberth and Fasullo 2008). Triangles indicate direct estimates with their uncertainty ranges from the 2009-2013 RAPID data (cyan), from Ganachaud and Wunsch 2003 (blue) and Lumpkin and Speer 2007 (magenta). (b) Times series of the total Atlantic MHT across 26.5° N as estimated by RAPID (blue), from GLOB16 (red) and GLOB4 (black).
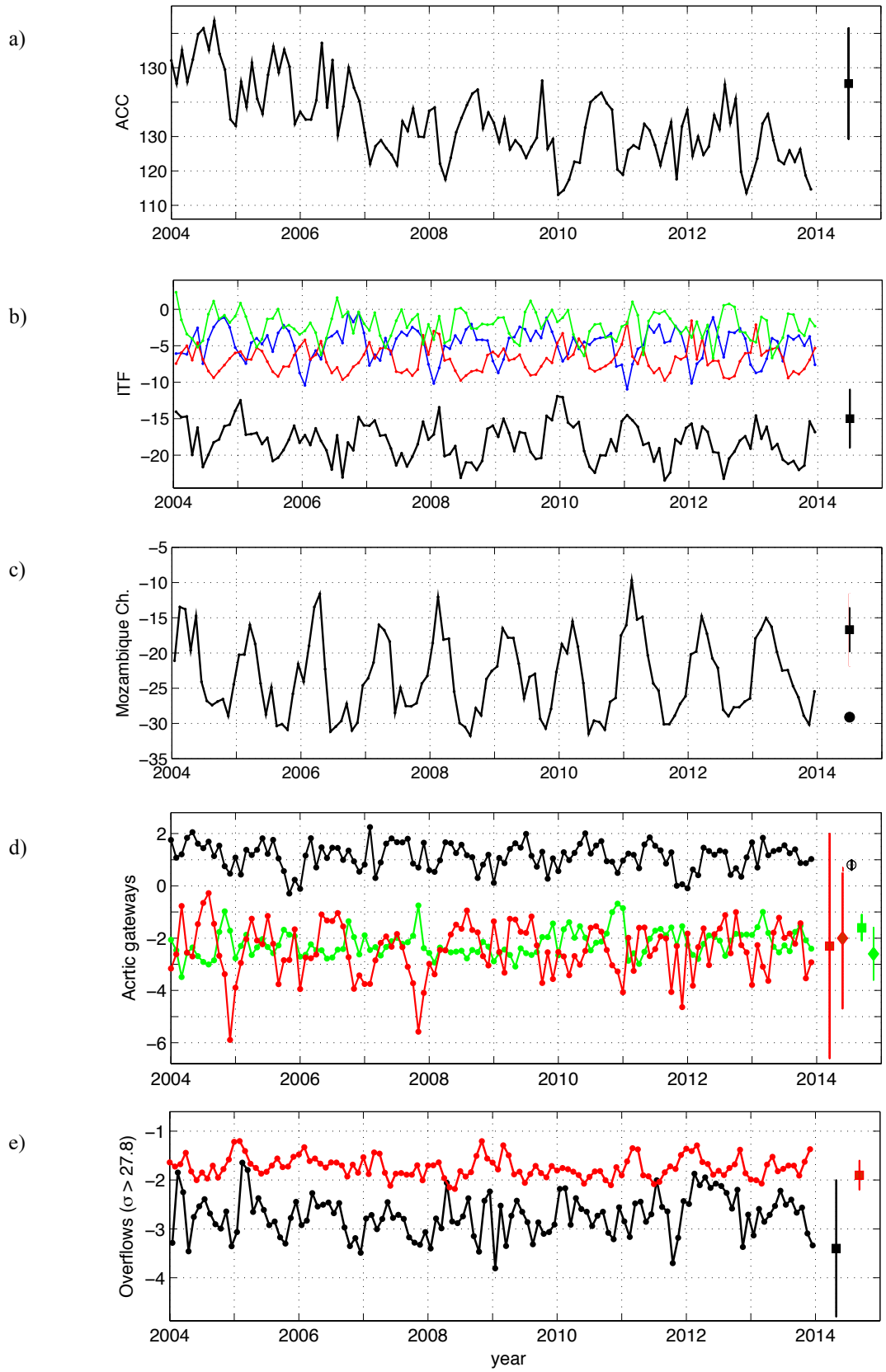
31

Fig. 5. Time series of the monthly averaged volume transport (in Sv) of the (a) ACC, (b) ITF (decomposed in Timor passage (red), Ombai strait (blue) and Lombok strait (green)), through the (c) Mozambique Channel, (d) Bering Strait (black), Fram Strait (red) and Davis Strait (green), and (e) for dense overflow through Denmark Strait (black) and Faroe Bank Channel (red). Observed values with error bars (as reported in Table 2) are shown.
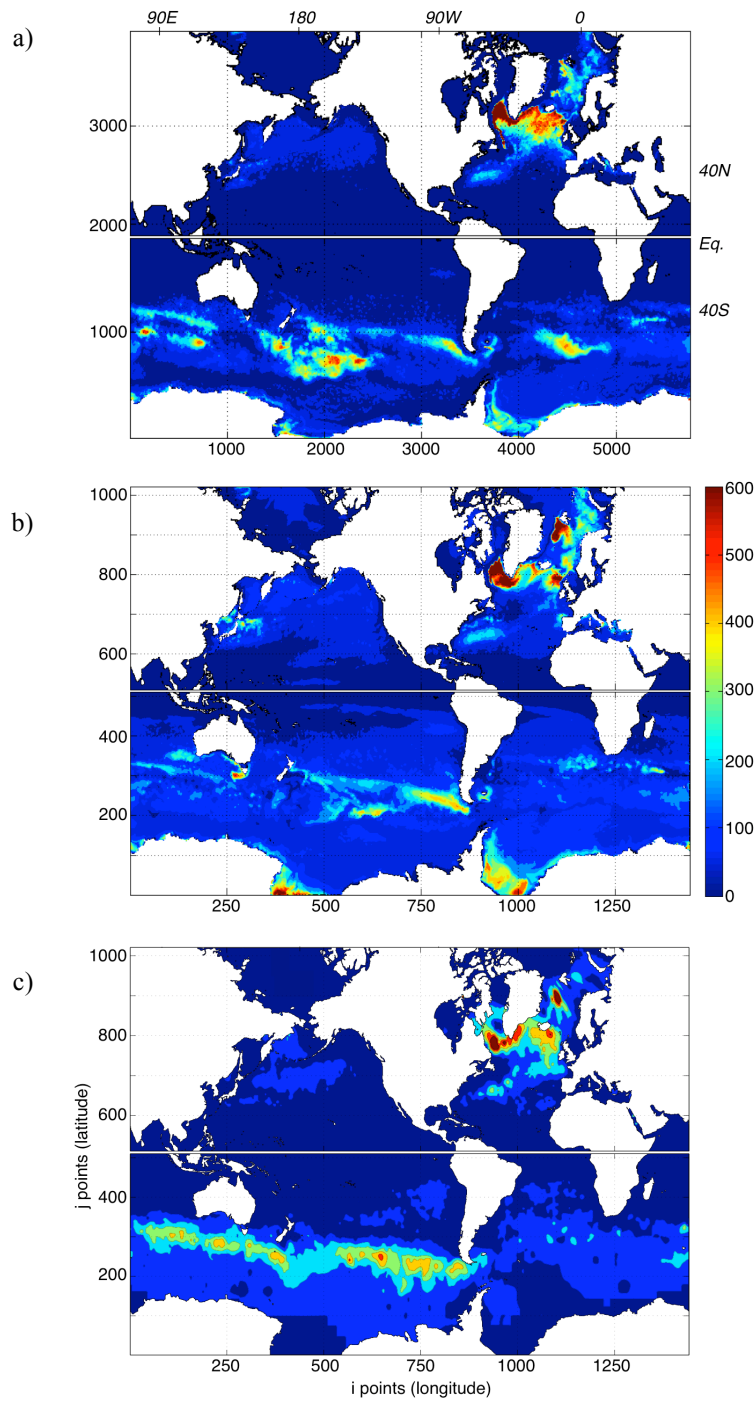
Fig. 6. (a) MLD (in m) averaged over March (in the Northern hemisphere) and September (in the Southern hemisphere) 2009-2013 from (a) GLOB16, (b) GLOB4, and (c) the de Boyer Montégut et al. (2004) climatology, based on a 0.03 threshold on density profiles. Model outputs are ~~is~~ shown on the native grid; observations are interpolated on the eddy-permitting ORCA grid. Numbers of grid points are indicated on the axis, along with indications of latitudes and longitudes.

33
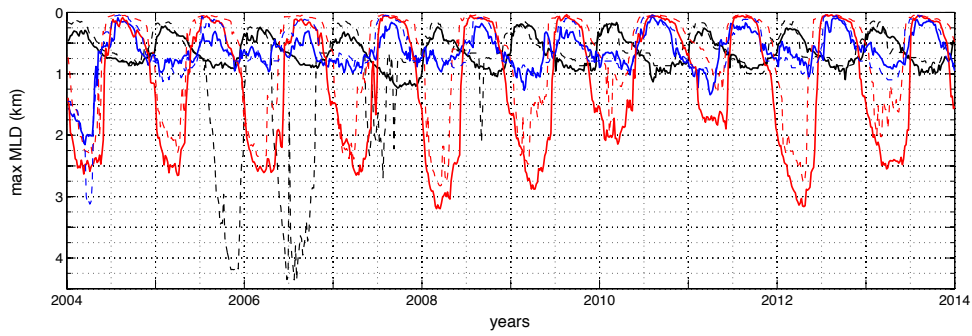
1
2 Fig. 7. Time series of modelled MLD maxima (in km) in the North Atlantic Ocean (red), the Nordic Seas (blue)
3 and the Southern Ocean (black) from GLOB16 (solid lines) and GLOB4 (dashed).
4
5
6
7
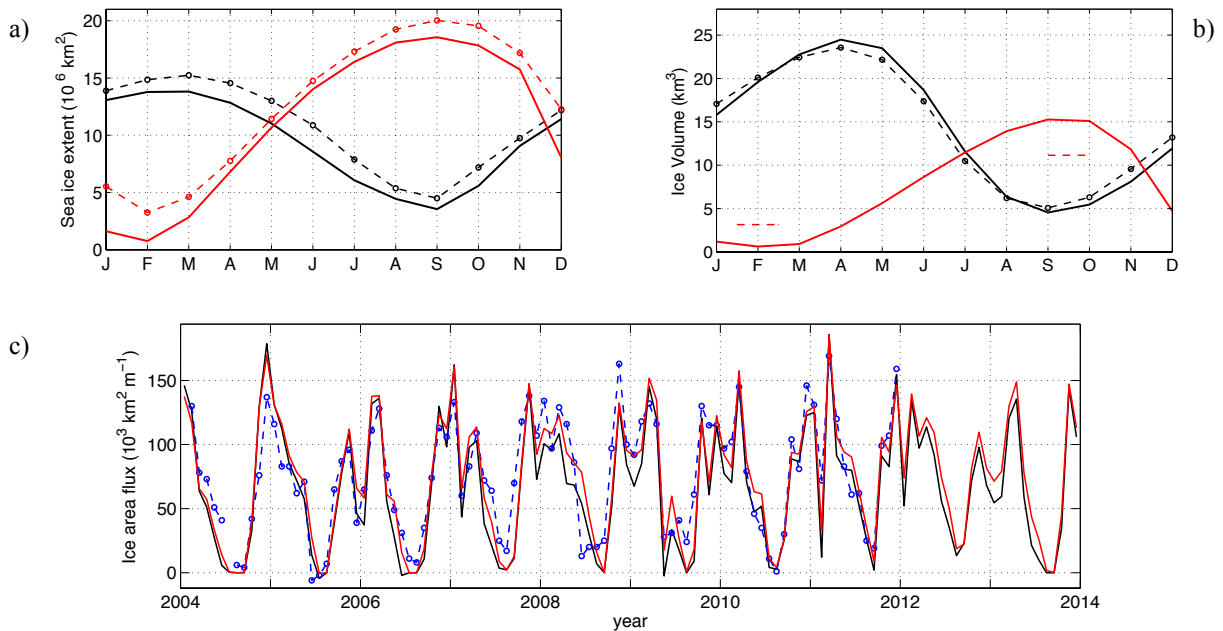
8 Fig. 8. (a) Mean GLOB16 seasonal cycles of sea ice extent (10^6 km^2) for the Arctic (black) and Antarctic (red)
9 oceans compared to satellite observations (dashed line) provided by NSIDC. Sea ice extent is defined as the area
10 enclosed in the 10% sea ice concentration contour. (b) Mean seasonal cycles of sea ice volume (10^3 km^3) for the
11 Arctic Ocean (black) compared to PIOMAS reanalysis (dashed line), and for the Antarctica (red) compared to
12 minimum and maximum values from ICESat. (c) Sea ice area export (10^3 km^2 month^{-1}) across Fram Strait for
13 GLOB16 (red), GLOB4 (black) and observations (blue).
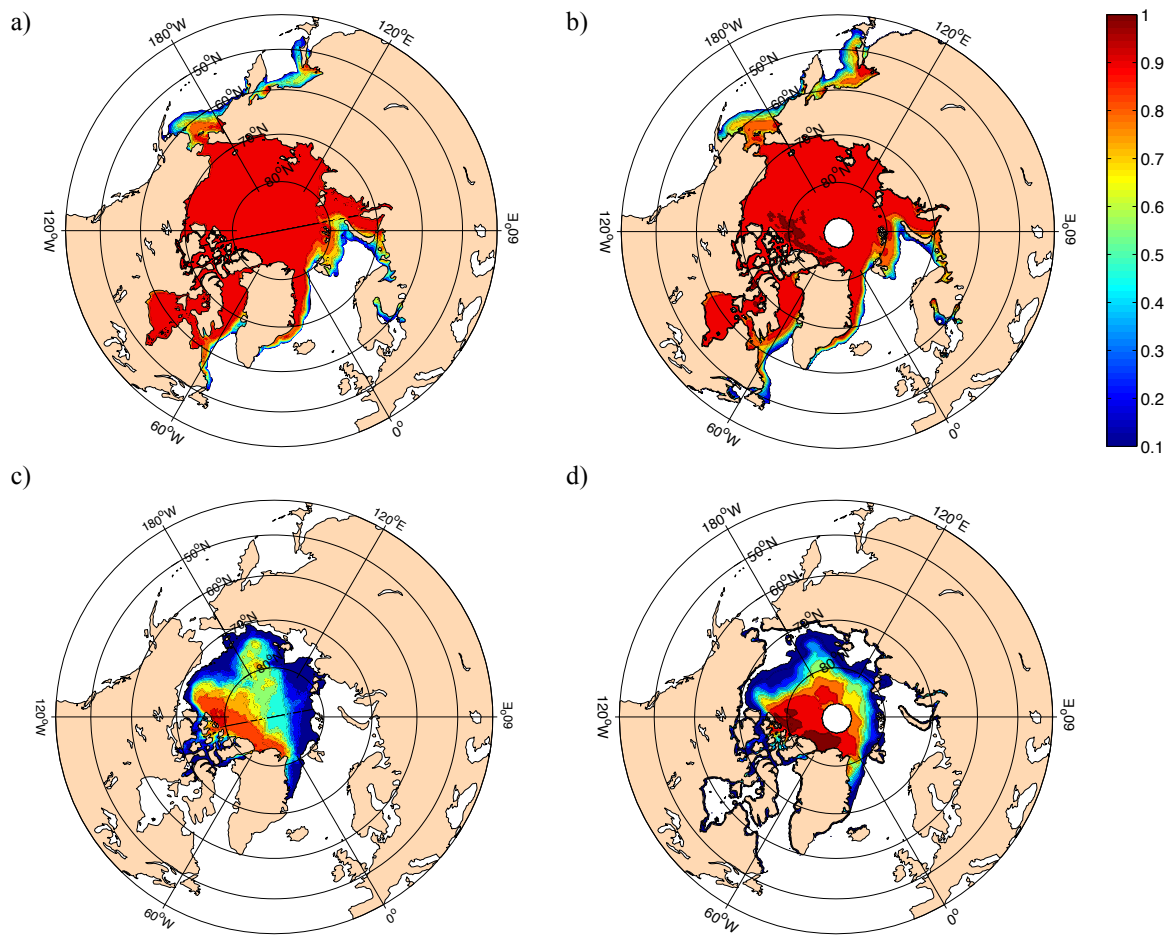
Fig. 9. Maximum (a, b) and minimum (c, d) Arctic sea ice concentration for the period 2009-2013 in GLOB16 (left) and observational data set (right).
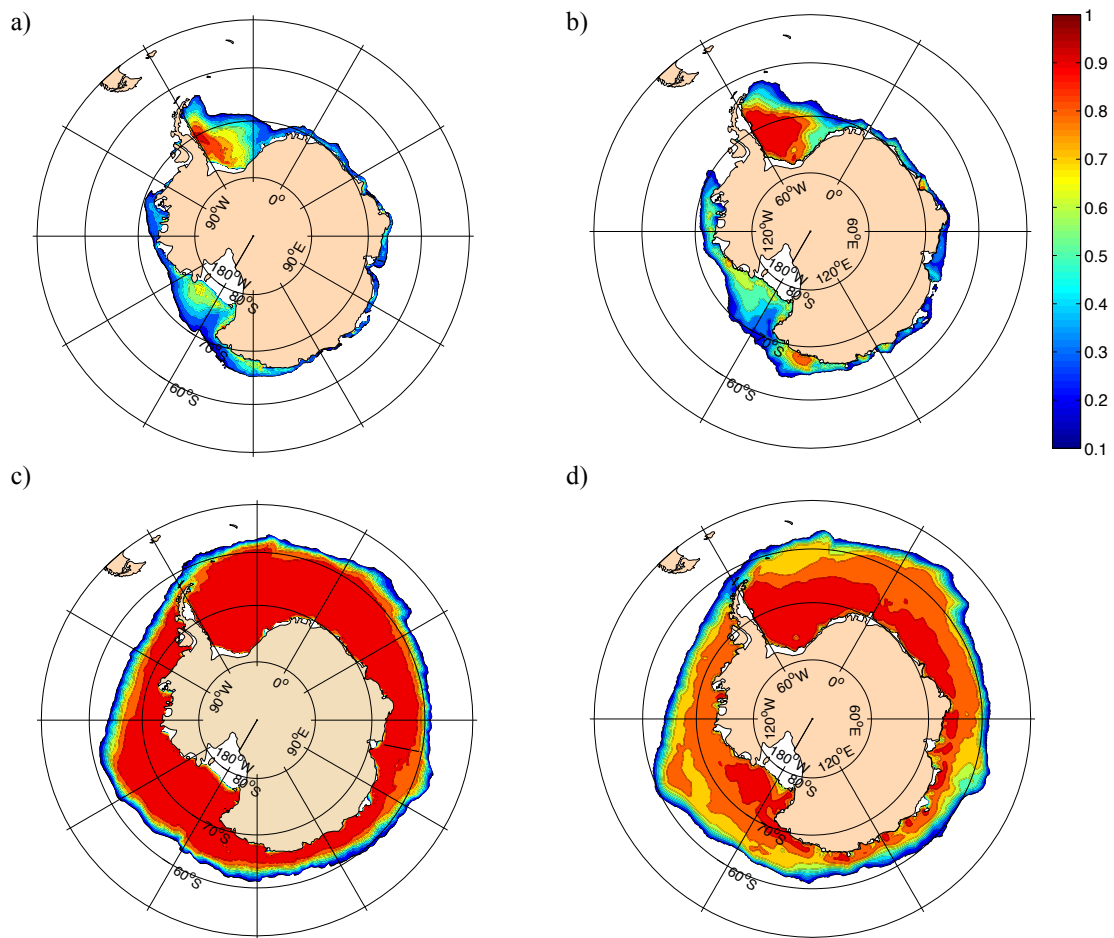
1   Fig. 10. Maximum (a, b) and minimum (c, d) Antarctic sea ice concentration for the period 2009-2013 in
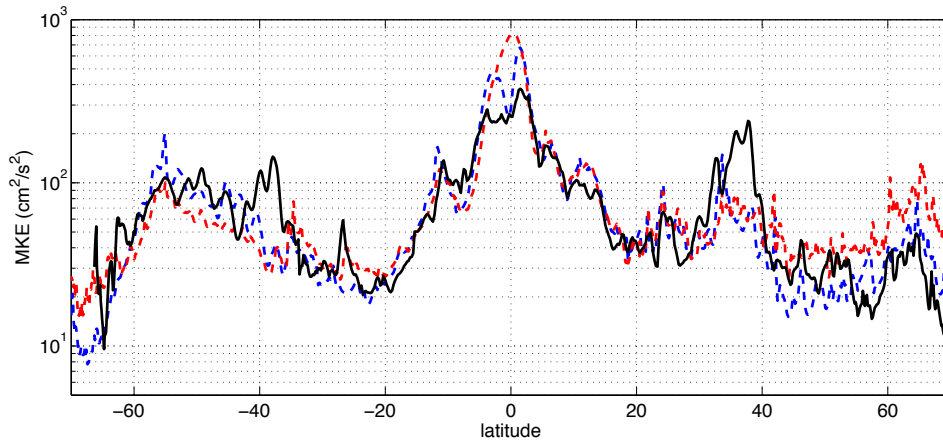2   GLOB16 (left) and observational data set (right).
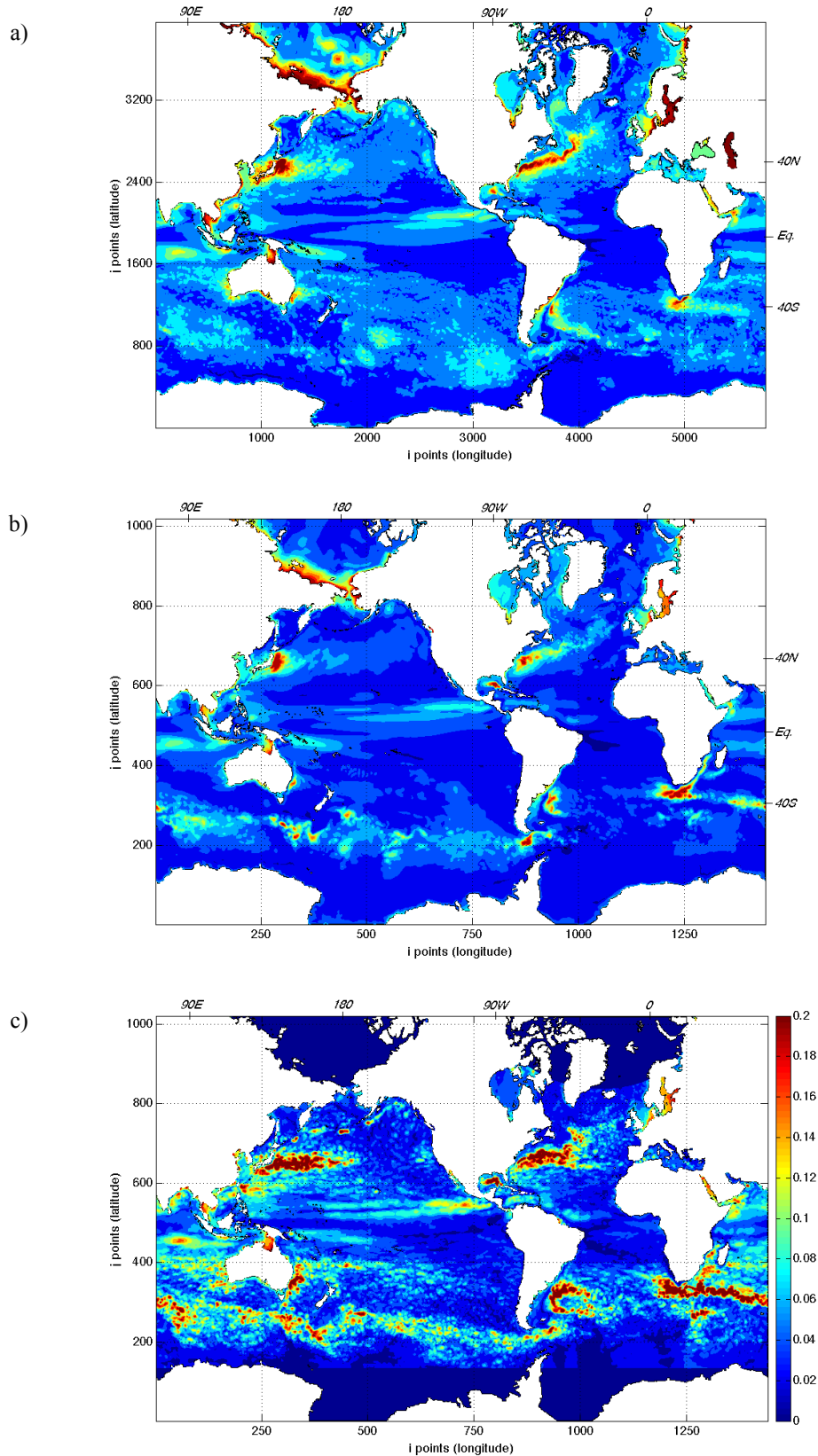
Fig. 11. Sea surface height variability (in m) from (a) the GLOB16 model, (b) the GLOB4 model and (c) AVISO. Modelled fields are shown on the own model grid; observations are interpolated on the eddy-permitting ORCA grid. Numbers of grid points are indicated on the axis, along with indications of latitudes and longitudes.
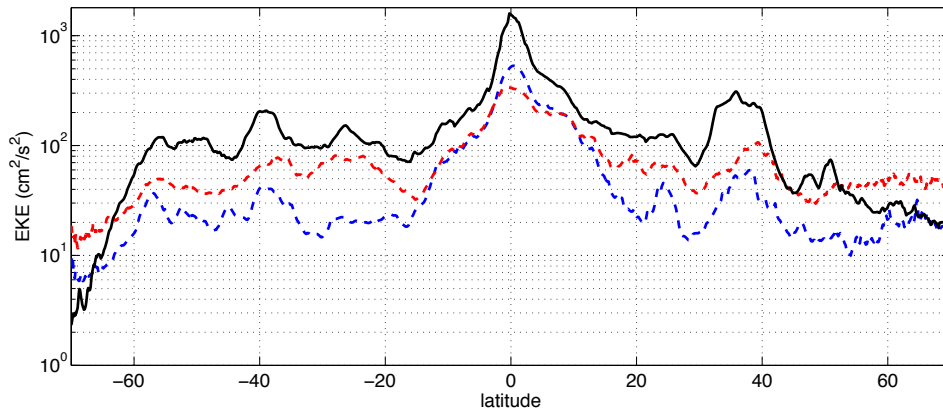
Fig. 12. (a) Latitudinal profiles of the global zonal-mean EKE (in cm^2 s^{-2}) of the surface flow for 2013 from GLOB16 (red), GLOB4 (blue) and OSCAR (black). Scale is logarithmic. (b) As (a), but for the MKE of the surface flow (in cm^2 s^{-2}).